

# Biohydrogen Production via Genetically Optimized Dual-Stage Fermentation with Directed CO<sub>2</sub> Capture and Biological Recycling: A Theoretical Framework

Rafsan Aziz Khan

Independent Researcher

ORCID: [0009-0004-7265-6778](https://orcid.org/0009-0004-7265-6778)

Email: [alhaitham017@gmail.com](mailto:alhaitham017@gmail.com)

## **Abstract**

Microbial hydrogen production presents a compelling alternative to conventional methods such as steam methane reforming and electrolysis, offering the potential for low-energy, carbon-conscious fuel generation. This theoretical study proposes a dual-stage hydrogen production system utilizing genetically optimized strains of *Clostridium butyricum* and *Rhodobacter sphaeroides* within a vertically integrated bioreactor. The system is designed to maximize hydrogen recovery through sequential dark fermentation and photofermentation, leveraging glucose as the primary substrate and water as an additional electron source.

Stoichiometric modelling of the full metabolic cycle predicts a hydrogen yield of **12 mol H<sub>2</sub> per mol of glucose**, representing the complete recovery of all hydrogen atoms available from the substrate and water. This equates to **13.45% yield by glucose mass, or 8.41%** when including **water input**. The design includes membrane-based gas separation and redirection of CO<sub>2</sub> emissions to biological sinks such as sugarcane plantations, bamboo forests, and algae bioreactors to enhance sustainability and carbon offset potential.

While experimental validation is pending, this model establishes an upper-bound theoretical framework for microbial hydrogen recovery and CO<sub>2</sub> integration. Emphasis is placed on idealized assumptions regarding enzyme function, microbial conversion efficiency, and gas capture. The results are intended to guide future research into scalable, decentralized biohydrogen platforms aligned with global climate goals.

(This model defines an idealized performance ceiling and includes realism-adjusted scenarios using expression and membrane correction factors.)

---

*Author's Note:* While this paper maintains a formal structure throughout, certain sections include personal reflections to transparently highlight the limitations and human considerations behind the model.

*Regarding System Clarity:* This paper presents a theoretical framework and does not include structural schematics, reactor diagrams, or CAD-level fabrication plans. The dual-stage metabolic system is described through stoichiometric equations, kinetic approximations, and structured yield modelling. While physical layout diagrams are excluded, all system components—fermentative stages, metabolic routing, gas separation, and CO<sub>2</sub> redirection—are captured via theoretical modelling. As this is a conceptual design, schematic representations are deferred to future experimental or engineering-focused work once biological viability is established.

---

## 1. Introduction

The transition to clean and sustainable energy sources remains one of the most urgent scientific challenges of the 21st century. Hydrogen has emerged as a promising candidate due to its high energy content and zero-emission profile at the point of use. However, current industrial hydrogen production methods—most notably steam methane reforming (SMR)—are carbon-intensive, heavily reliant on fossil fuels, and contribute substantially to greenhouse gas emissions. While water electrolysis offers a cleaner alternative, it is hindered by high energy requirements and dependence on renewable electricity infrastructure, limiting its scalability—particularly in regions with limited access to renewable energy systems.

Biological hydrogen production through microbial fermentation has gained increasing attention as a low-energy, renewable pathway. Specific strains such as *Clostridium butyricum* and *Rhodobacter sphaeroides* can convert organic substrates into hydrogen gas under anaerobic conditions. Dark fermentation using *C. butyricum* can rapidly degrade sugars like glucose into hydrogen and volatile fatty acids, while photofermentation by *R. sphaeroides* enables the further conversion of these acids—particularly butyric and acetic acid—into additional hydrogen using light energy. In addition to carbon-based substrates, water molecules serve as critical electron donors during photofermentation, providing the oxygen atoms released as carbon dioxide and the protons required for sustained hydrogen generation.

Despite their promise, single-stage microbial systems are typically limited by incomplete substrate utilization, accumulation of metabolic byproducts, and suboptimal hydrogen yields. This paper proposes a dual-stage hydrogen production model that integrates genetically optimized strains of *C. butyricum* and *R. sphaeroides* in a vertically structured bioreactor. By coupling dark fermentation with downstream photofermentation, the system aims to maximize hydrogen recovery from both glucose and its metabolic derivatives. Genetic modifications are introduced to enhance hydrogenase activity, reduce competing metabolic fluxes, and improve light harvesting under low-intensity conditions.

In addition to yield optimization, the system incorporates a membrane-based gas separation unit to extract and isolate carbon dioxide produced during fermentation. Rather than storing or releasing this CO<sub>2</sub>, the model proposes redirecting it to external biological systems—such as algae bioreactors, sugarcane plantations, or bamboo forests—for natural carbon sequestration and glucose regeneration. This combined approach aims to support the development of a decentralized, low-emission hydrogen production platform that aligns with global sustainability goals.

This study not only proposes a theoretical biohydrogen system but also introduces a time-resolved kinetic modelling framework to simulate microbial reaction rates and predict real-time behaviour. Additionally, it incorporates a carbon sequestration strategy via high-efficiency C<sub>4</sub> crop integration, allowing passive redirection of emitted CO<sub>2</sub> into a sugarcane-based sink. These elements collectively enhance the model's viability for real-world deployment.

## 2. Methodology and Theoretical Modelling Framework

This study employs a layered theoretical modelling approach to simulate microbial hydrogen production via a genetically optimized dual-stage fermentation system. As the model is conceptual and not experimentally validated, the methodology emphasizes stoichiometric yield estimation, metabolic pathway design, kinetic approximation, and energy budgeting under idealized constraints. The following components define the modelling framework:

### 2.1. Stoichiometric Modelling

Hydrogen yield predictions are derived from balanced metabolic equations for *Clostridium butyricum* (dark fermentation) and *Rhodobacter sphaeroides* (photofermentation). Mass- and mole-based hydrogen outputs are calculated using standard molar masses under complete substrate conversion assumptions.

### 2.2. Genetic Engineering Assumptions

Proposed genetic modifications are modelled as fully functional and chromosomally integrated. Edits such as overexpression of hydrogenases and metabolic enzymes or gene knockouts are based on documented literature. The model assumes no expression instability, mutation, or metabolic burden, representing best-case functional performance.

### 2.3. Bioreactor Design Assumptions

The reactor is conceptualized as a vertically integrated, gravity-assisted dual-chamber system with scaffold-supported microbial biofilms. Mass transfer of VFAs between stages is passive. Each chamber operates under fixed environmental conditions (anaerobic, temperature-stabilized), with light access provided for the photofermentative stage. Uniform biofilm structure, metabolite diffusion, and chamber isolation are assumed.

### 2.4. Kinetic Approximations

Microbial activity is modelled using Monod kinetics for glucose consumption and light-saturation kinetics for photofermentation. Empirical constants are adapted from published literature. These models provide time-based performance insights but are not calibrated to experimental data.

#### Important Note on Hydrogen Feedback Inhibition:

While this model simulates microbial kinetics under ideal extraction conditions, it does not account for enzymatic inhibition due to hydrogen accumulation in the reactor headspace. Literature reports show that hydrogenase and nitrogenase activity in *C. butyricum* and *R. sphaeroides* respectively are suppressed at H<sub>2</sub> partial pressures >0.6–0.8 atm. This inhibition can significantly reduce gas output in poorly ventilated systems. Future kinetic models should incorporate dynamic headspace gas modelling and feedback inhibition thresholds for accurate time-course prediction.

## 2.5. Energy and Cost Calculations

Energy requirements for illumination, gas extraction, and basic control systems are estimated using power consumption values from typical lab-scale equipment. Hydrogen output energy is calculated using the combustion enthalpy of H<sub>2</sub> (286 kJ/mol). Cost analysis is based on U.S. bulk pricing for glucose, amortized component use, and power rates, reflecting theoretical minimums.

*(All pricing references are based on pre-2020 U.S. bulk rates, before tariff-induced market distortions introduced under Trump's presidency. This ensures pricing reflects commodity baselines unaffected by policy-driven inflation.)*

## 2.6. Gas Separation and CO<sub>2</sub> Routing

A vacuum-assisted membrane system is modelled with perfect hydrogen/CO<sub>2</sub> separation efficiency, no fouling, and lossless operation. Separated CO<sub>2</sub> is routed to sugarcane-based sinks via passive or root-zone injection. Biological sinks are assumed to operate at full fixation capacity with no lag or underperformance.

### Author's Note on Electrochemical Capture Alternatives:

During the modelling phase, I reviewed electrochemical CO<sub>2</sub> capture approaches such as the fluoquinone-based FFDS redox system [Wei et al., 2025], which offers oxygen-tolerant operation and reversible capture via pH-swing chemistry. While conceptually interesting, I found the overall energy-to-capture ratio and CO<sub>2</sub> managing cycle to be suboptimal for integration into this system. In particular, the reliance on high energy input without a built-in utilization path renders it inefficient when compared to biological fixation strategies.

Therefore, this model intentionally favours photosynthetically active CO<sub>2</sub> sinks—namely sugarcane plantations and algae bioreactors—which not only sequester CO<sub>2</sub> passively but regenerate glucose substrates for further biohydrogen production. Unless future work demonstrates a tightly coupled valorisation pathway for electrochemically captured CO<sub>2</sub>, I consider this class of sorbents unsuitable for the present system.

## 2.7. Scope Limitations

This framework assumes ideal substrate purity, enzyme functionality, membrane integrity, and microbial behaviour. Stochastic variability, environmental drift, and hardware degradation are not included. These simplifications serve to define a theoretical upper-bound system performance.

This section consolidates the modelling strategies underlying the theoretical framework, ensuring clarity and reproducibility for future studies. While certain sections of the paper include personal reflections to contextualize design constraints, the scientific modelling remains rigorous and idealized for conceptual benchmarking.

## 2.8. Assumptions Tiers and Realism Factors

To clearly delineate the scope of this theoretical model, all system assumptions are categorized by domain and impact severity. While idealized conditions are necessary to establish a performance ceiling, this section outlines the tiers of assumptions applied and proposes adjustments for more realistic modelling.

Assumptions are grouped into four tiers—**structural**, **biological**, **engineering**, and **environmental**—each with distinct implications for system behaviour and model reliability.

Tier	Assumption Type	Examples	Treatment
Tier 1 – Structural	Gravity-fed VFA transfer, scaffold-stable biofilms, anaerobic integrity	Accepted for conceptual clarity	Supported by bench-scale analogues, but flow obstruction and gradient formation likely in real systems
Tier 2 – Biological	100% enzyme expression, no mutation, full substrate conversion, no biomass loss	Idealized; adjustable using Biological Realism Factor (BRF)	Literature supports 10–25% expression drop over time; real-world BRF = 0.75–0.90
Tier 3 – Engineering	Perfect membrane separation (100% H <sub>2</sub> /CO <sub>2</sub> split), zero fouling, no vacuum loss	Accepted for theoretical benchmarking	Real systems show 85–95% separation efficiency with membrane aging and backpressure; fouling mitigation required
Tier 4 – Environmental	Continuous CO <sub>2</sub> fixation by sugarcane, zero plant stress, no uptake lag	Assumed for CO <sub>2</sub> neutrality model	Real-world uptake is climate- and growth-phase-dependent; sequestration efficiency highly variable

To account for biological and engineering variability, the **Biological Realism Factor (BRF)** is introduced as a global modifier. This factor adjusts theoretical hydrogen yields and gas separation performance downward based on expected losses in enzyme expression, cofactor depletion, metabolic burden, and system wear.

Typical BRF values based on published microbial expression data range from **0.75 to 0.90**, depending on strain, expression system, and cultivation duration. All future yield, energy, and cost calculations in this paper can be scaled using this factor to reflect more realistic operating envelopes.

All core values can be scaled by the BRF for realism-adjusted estimates. Tables in Sections 9 and 14 reflect uncorrected theoretical ceilings; adjusted versions appear alongside them for realistic comparison.

The tiered structure also supports future scenario modelling—allowing researchers to evaluate system resilience under degraded conditions, such as partial membrane failure, incomplete VFA conversion, or temporary CO<sub>2</sub> sink inoperability.

### 2.8.1. Realism Adjustment Factors and Modelling Scope

To quantitatively bridge the gap between idealized assumptions and real-world system behaviour, this model introduces a set of realism adjustment factors. Each factor targets a specific constraint domain—biological, genetic, engineering, or metabolic—allowing theoretical outputs to be scaled toward plausible operating ranges. These factors serve as modular modifiers for sensitivity analysis, scenario modelling, and future experimental calibration. This table summarizes the core factors used throughout this study.

Factor	Full Name	Purpose	Typical Range	Applied In
<b>BRF</b>	Biological Realism Factor	Adjusts for enzyme expression loss, mutation, and metabolic burden	0.75 – 0.90	H <sub>2</sub> yield, cofactor availability
<b>GSCF</b>	Gene Stack Correction Factor	Reduces yield due to combinatorial gene expression overload	0.6 – 0.9	Total H <sub>2</sub> yield per cycle
<b>MFCF</b>	Membrane Flux Correction Factor	Compensates for real-world limitations in gas extraction throughput	0.7 – 0.85	Effective H <sub>2</sub> recovery vs. inhibition
<b>BDF</b>	Biomass Diversion Factor	Represents substrate carbon diverted to biomass instead of gas	0 – 30%	Net CO <sub>2</sub> & H <sub>2</sub> output, system efficiency

*Side Note:* Each factor provides a correction pathway from the theoretical ceiling toward a more biologically and operationally plausible scenario. These modifiers allow the model to scale across research environments—from ideal lab conditions to pilot-scale deployments.

## 2.9 Core Parameter Reference Table

This table consolidates key assumptions, constants, and system parameters used throughout the model for ease of cross-reference.

Parameter	Value	Units	Context/Notes
Molar mass of glucose	180.16	g/mol	Primary substrate
Molar mass of water	18.015	g/mol	Photofermentation donor
Molar mass of H <sub>2</sub>	2.02	g/mol	For mass yield
H <sub>2</sub> energy content	286	kJ/mol	Based on combustion enthalpy
H <sub>2</sub> yield per cycle	12	mol	Theoretical max (6 from glucose, 6 from water)
CO <sub>2</sub> output per cycle	6	mol	2 from dark, 4 from photofermentation
Membrane separation efficiency	92	%	Real-world polymer-MOF hybrid estimate
LED light intensity	30	μmol/m <sup>2</sup> /s	Minimum needed for nitrogenase activation
Nitrogenase ATP cost	20	mol ATP/mol H <sub>2</sub>	Average demand estimate
Vacuum pump energy	216	kJ/cycle	30 W for 2 hours
Total input energy	960	kJ/cycle	Including LED + mixing + control
BRF range	0.75–0.90	-	Adjusts for biological inefficiencies
BDF range	0–30	%	Represents substrate diverted to biomass
Areal light requirement	≥0.02	m <sup>2</sup> per L	Minimum surface exposure for photofermentation
Photofermentative H <sub>2</sub> yield	10	Mol	From 1 mol butyric acid + 6 mol water
Effective efficiency (realistic)	40–60	%	Total system, biologically corrected
H <sub>2</sub> volume per cycle	~89.7	-	At STP, for 12 mol H <sub>2</sub>

### Consistency Notes on STP Assumptions

All gas volumes reported in this paper are assumed to be measured under **Standard Temperature and Pressure (STP)** conditions (1 atm, 273.15 K), unless otherwise specified. This standardization ensures comparability across reported hydrogen yields, especially in volumetric metrics.



## Terminology Reference Table

To ensure clarity throughout this paper, the following standardized terminology is adopted:

Term	Definition	Usage Context
<b>Theoretical Ceiling</b>	The maximum yield or performance achievable under idealized biological and engineering conditions. Assumes perfect enzyme expression, complete substrate conversion, and zero system losses.	Used for defining best-case outputs in stoichiometric and energy models.
<b>Idealized Model</b>	A conceptual model that excludes stochastic effects, degradation, or regulatory limitations. Used to benchmark the system's theoretical potential.	Applied in early-stage modelling (Sections 2–5).
<b>Realistic Scenario</b>	A model adjusted using Biological Realism Factor (BRF) and Biomass Diversion Factor (BDF) to account for expression loss, cofactor limitations, and carbon retention.	Applied in Sections 8.3–9 for grounded yield and efficiency estimates.
<b>Yield by Mass</b>	Percentage of hydrogen mass relative to input substrate mass. Contextualized against either glucose-only, glucose + water, or butyrate + water.	Standard in biochemical literature (Sections 3, 8).
<b>Energy Yield</b>	Total energy output from H <sub>2</sub> combustion (in kJ or MJ), based on molar hydrogen production.	Used for benchmarking system viability and efficiency (Section 9).
<b>Volumetric Productivity</b>	Hydrogen output per litre of reactor volume per day (L/L/day).	Used for scaling comparisons in fermentation systems (Section 10).
<b>Areal Productivity</b>	Hydrogen output per square meter of light-exposed surface area per day (L/m <sup>2</sup> /day).	Used to evaluate light-limited photofermentation stages (Section 5.2.1).

*Side Note:* Throughout this paper, "Theoretical Ceiling" and "Idealized Model" are used interchangeably to describe system performance under best-case assumptions. Where realistic corrections are applied, these are explicitly tagged using BRF and BDF modifiers.



### 3. Biochemical Pathways and Theoretical Yield Modelling

Hydrogen production through microbial metabolism is driven by a series of enzymatically regulated biochemical pathways, with stoichiometric constraints that define the theoretical maximum yields achievable from specific substrates. This section models the metabolic pathways of two key microorganisms—*Clostridium butyricum* and *Rhodobacter sphaeroides*—within the context of a dual-stage fermentation system. Yield calculations are based on molar balances and mass conversions to assess the energy potential and gas output of the proposed design.

#### 3.1. Dark Fermentation Pathway (*Clostridium butyricum*)

Dark fermentation is an anaerobic process wherein glucose is catabolized to yield hydrogen gas, carbon dioxide, and volatile fatty acids (VFAs), primarily butyric and acetic acids. The simplified stoichiometric reaction is as follows:



##### 3.1.1. Theoretical Hydrogen Yield Calculation:

- Molar mass of glucose ( $\text{C}_6\text{H}_{12}\text{O}_6$ ): 180.16 g/mol
- Molar mass of hydrogen ( $\text{H}_2$ ): 2.02 g/mol
- 2 mol  $\text{H}_2$  = 4.04 g hydrogen per mole glucose
- Yield by mass =  $\left(\frac{4.04}{180.16}\right) \times 100 \approx 2.24\%$

Key Enzymes:

- Glycolysis: Glucose  $\rightarrow$  Pyruvate
- Pyruvate:ferredoxin oxidoreductase: Pyruvate  $\rightarrow$  Acetyl-CoA +  $\text{CO}_2$  + reduced ferredoxin
- [FeFe]-Hydrogenase: Reduced ferredoxin  $\rightarrow$   $\text{H}_2$

#### 3.2. Photofermentation Pathway (*Rhodobacter sphaeroides*)

In the second stage, *R. sphaeroides* photoferments VFAs under anaerobic, light-activated conditions to produce additional hydrogen. A representative reaction using butyric acid is:



The representative stoichiometric reaction for photofermentation used in this model reflects the complete oxidation of butyric acid under idealized conditions. This formulation aligns with theoretical yields reported in prior photofermentation studies, where yields of up to 10 mol  $\text{H}_2$  per mol of butyrate have been proposed based on full hydrogen atom recovery from both the substrate and water-derived protons. Notably, studies by Ghosh and Hallenbeck (2010) and Nath & Das (2004) support theoretical ceilings in the 8–10 mol  $\text{H}_2$  range when nitrogenase is fully activated and substrate inhibition is minimal. These values serve as a theoretical upper limit and are not typically achieved in practical systems, where reported yields range from 5.6 to 7.8 mol  $\text{H}_2$ /mol butyrate due to cofactor limitations, metabolic branching, and photon attenuation.

### 3.2.1. Theoretical Hydrogen Yield Calculation:

- Molar mass of butyric acid ( $C_4H_8O_2$ ): 88.11 g/mol
- 10 mol  $H_2$  = 20.2 g hydrogen per mole butyric acid
- Total mass input = 88.11 + 108.09 = 196.2 g
- Yield percentage =  $\left(\frac{20.2}{196.2}\right) \times 100 \approx 10.29\%$  **by mass**

Key Components:

- Light-harvesting complexes (LH1, LH2)
- Nitrogenase enzyme (light activated, ATP-dependant)
- Electron donors: reduced Ferredoxin and NAD(P)H

*Side Note:* While the yield of 10 mol  $H_2$  per mol butyric acid represents the full theoretical recovery of all hydrogen atoms, experimental photofermentation systems commonly achieve yields between 5.6 and 7.8 mol  $H_2$  per mol substrate due to energy losses, biomass generation, and metabolic branch pathways [2,3]. This model assumes full oxidation as a theoretical ceiling and excludes these real-world constraints.

### Real-World Photofermentation Ceiling Adjustment

While the 10 mol  $H_2$  per mol butyrate value used in this model aligns with theoretical maximums reported in prior photofermentation studies [Ghosh & Hallenbeck, 2010; Nath & Das, 2004], real-world yields are consistently lower due to kinetic constraints, light attenuation, cofactor scarcity, and regulatory bottlenecks. Most experimental setups report practical ranges of 5.6–7.8 mol  $H_2$ /mol butyrate under optimized but realistic conditions.

To reflect this discrepancy, a corrected yield range is proposed below. These values can be used to recalibrate energy output, system efficiency, and  $CO_2$  generation when evaluating real-world deployment scenarios:

Metric	Ideal	Realistic (7 mol)	Realistic (5.6 mol)
$H_2$ per mol butyrate	10 mol	7 mol	5.6 mol
Total $H_2$ per cycle	12 mol	9 mol	7.6 mol
Energy Output	3432 kJ	2574 kJ	2174 kJ
Net Energy Gain	2472 kJ	1614 kJ	1214 kJ
Efficiency (EROIE)	3.58	2.68	2.26

This yield gradient reinforces the importance of integrating Biological Realism Factor (BRF) and cofactor correction layers into all performance metrics, rather than relying solely on stoichiometric ceilings. Future reactor designs should benchmark against the 7 mol case unless continuous light optimization and genetic stabilization are proven experimentally.

### 3.3. Overall Hydrogen Yield from One Cycle

Assuming complete substrate conversion in both stages:

From 1 mol of glucose and 6 mol of water, the system yields a total of 12 mol of hydrogen—recovering 6 mol from glucose-derived metabolites and 6 mol from water-derived protons via photofermentation. This distribution reflects full hydrogen recovery from both the substrate and external electron donor sources. This corresponds to mass-based yields of 13.45% relative to glucose alone, and 8.41% when water input is included. Presenting both molar and mass-based values provides clarity on yield interpretation across biochemical and engineering contexts.

*Side note:* This yield assumes full constructive collaboration across all genetic edits. Applying a GSCF of 0.75–0.9 reduces this to 9–10.8 mol under more realistic gene stack limits.

#### H<sub>2</sub> Volume Clarification:

All hydrogen volume calculations throughout this model assume **Standard Temperature and Pressure (STP)** conditions—specifically, 1 atm pressure and 273.15 K (0°C). Under these parameters, one mole of an ideal gas occupies 22.414 litres. Thus, the 12 mol H<sub>2</sub> yield per cycle corresponds to approximately **268.97 litres of gas at STP**. This value scales linearly with reactor operation and can be recalculated for non-STP conditions using the ideal gas law ( $PV = nRT$ ). All real-world volume estimates should incorporate system temperature and backpressure to avoid yield inflation.

H <sub>2</sub> Source	Origin Compound	Hydrogen Atoms Contributed	Mol H <sub>2</sub> Equivalent	Note
Glucose	Direct Substrate	12	6	Via dark fermentation (partial) and VFA-based photofermentation
Water	Electron Donor in Photofermentation	12	6	Split via light-driven nitrogenase pathway
Total		24	12	Mass balance validated

For yield definitions (mass yield, energy yield, productivity), see the table in Section 8.0.2.

#### 3.3.1. Hydrogen Atom Origin Clarification

This breakdown aligns with mass balance and theoretical atom conservation. This ensures mass conservation is maintained and avoids misinterpretation of hydrogen recovery calculations.

Reaction Stage	Input Molecule(s)	Process	Hydrogen Atoms Contributed	Mol H <sub>2</sub> Generated
Dark Fermentation	1 mol Glucose	Glycolysis → VFAs + H <sub>2</sub>	4 atoms	2 mol
Photofermentation	1 mol Butyric Acid (from glucose) + 6 mol	Light-driven nitrogenase activity	20 atoms	10 mol
Total			24 atoms	12 mol

*Side Note:* Glucose alone could at most yield 6 mol H<sub>2</sub> if fully oxidized for its 12 H atoms. The additional 6 mol in this model derive from photobiological water splitting.

### 3.4. CO<sub>2</sub> Generation Summary

- Dark fermentation: 2 mol CO<sub>2</sub>
- Photofermentation: 4 mol CO<sub>2</sub>
- Total = 6 mol CO<sub>2</sub> per mol glucose
- Molar mass of CO<sub>2</sub> = 44.01 g/mol
- Total CO<sub>2</sub> mass = 264.06 g per cycle
- CO<sub>2</sub>-to-glucose mass ratio = **146.56%**

#### Clarification on Carbon Flow and CO<sub>2</sub> Mass Output:

The CO<sub>2</sub>-to-glucose mass ratio of 146.56% reflects not an increase in carbon atoms, but rather the combined effects of **complete substrate oxidation** and the incorporation of **oxygen atoms from water** during photofermentation. Under ideal conditions, all six carbon atoms from glucose are oxidized—two during dark fermentation and four during photofermentation—yielding 6 mol of CO<sub>2</sub>.

However, when **biomass diversion** occurs (modelled via the **Biomass Diversion Factor, BDF**), a fraction of glucose-derived carbon is retained in microbial biomass instead of being oxidized. Since CO<sub>2</sub> production is tightly coupled to substrate oxidation—particularly in photofermentation—this diversion results in a **direct reduction in CO<sub>2</sub> output** and, by extension, a proportional drop in H<sub>2</sub> yield.

Therefore, this 146.56% ratio applies only under idealized, full-oxidation scenarios. In realistic systems, both CO<sub>2</sub> evolution and hydrogen production will decline according to the degree of biomass carbon retention.

### 3.5. Substrate Input Modelling and Real-World Substitution (Clostridium)

The hydrogen production efficiency of the dark fermentation stage depends directly on the availability of fermentable sugars. In this system, **Clostridium butyricum** operates as the primary anaerobic fermenter, converting sugars into hydrogen and volatile fatty acids (VFAs). To maintain continuous biohydrogen production, glucose feeding must ideally match the metabolic capacity of the biomass. The following assumptions are made under idealized conditions of substrate availability, metabolic activity, and conversion efficiency.

#### Biomass-Specific Glucose Consumption Rate

From literature and validated fermentation data:

- Specific glucose uptake rate of *Clostridium butyricum* (q<sub>s</sub>) ≈ **10 mmol/g biomass/hr**
- Molar mass of glucose (C<sub>6</sub>H<sub>12</sub>O<sub>6</sub>) = **180.16 g/mol**

Assuming full metabolic activity and no substrate inhibition, for a reactor with **15 g/L biomass concentration**, the hourly glucose requirement is:

$$q_s = 15 \text{ g/L} \times 10 \frac{\text{mmol}}{\text{g} \cdot \text{hr}} = 150 \text{ mmol/hr} = 0.15 \text{ mol/hr}$$

$$0.15 \text{ mol/hr} \times 180.16 \text{ g/mol} = 27.02 \text{ g/hr of glucose}$$

### Daily Glucose Requirement

$$27.02 \text{ g/hr} \times 24 \text{ hr} = 648.48 \text{ g/day of glucose}$$

Thus, assuming consistent uptake over a 24-hour cycle, a 1 L Clostridium chamber operating at 15 g/L biomass would theoretically require approximately **648 g of glucose per day**.

### Sugarcane Extract as a Substrate

To simulate real-world conditions, laboratory-grade glucose can be substituted with **sugarcane extract**, a cost-effective and renewable carbohydrate source.

**Average composition of sugarcane extract** (assumed):

- Total sugars: ~15% (150 g/L)
- Composition: ~75% sucrose, ~12% glucose, ~13% fructose

Given that the Clostridium strain has been genetically modified to metabolize **sucrose, glucose, and fructose**, it is assumed that the entire sugar content becomes fermentable without inhibition or metabolic bottleneck.

### Required Volume of Sugarcane Extract

$$\frac{648 \text{ g/day of fermentable sugar}}{150 \text{ g/day of sugarcane extract}} = 4.32 \text{ L/day}$$

### Final Estimation (Assumed Conditions)

Under idealized assumptions of full enzymatic activity, no feedback inhibition, and complete sugar utilization, a 1 L Clostridium reactor with 15 g/L biomass is expected to require:

- **648 g/day of pure glucose**, or
- **4.32 L/day of raw sugarcane extract** (15% w/v sugar concentration)

This calculation serves as a theoretical baseline for substrate supply and must be adjusted in practical systems to account for process inefficiencies, microbial adaptation lag, or variations in sugar concentration and extract purity.

### 3.6. Process Assumption

Parameter	Value	Justification
Glucose purity	100%	Ideal condition
Reactor temperature	37°C	Optimal for both organisms
Anaerobic Conditions	Strict	Necessary for both fermentation stages; oxygen presence inhibits key enzymes
Light intensity	30 $\mu\text{mol}/\text{m}^2/\text{s}$	Low, continuous light ( $\sim 30 \mu\text{mol}/\text{m}^2/\text{s}$ ) ensures constant nitrogenase activation
Complete substrate conversion	Yes	Assumes full conversion of glucose to VFAs, and VFAs to $\text{H}_2$ , under ideal conditions
Water availability	Excess	Water is available and maintained at 37°C, optimal for both strains
Genetic enhancements	Functional	Assumes overexpression is successful and stable, with no mutation or loss
No microbial cross-contamination	True	Each microbial population functions independently without inhibitory interactions

#### 3.6.1. Biomass Diversion Factor (BDF):

In realistic systems, 5–30% of substrate carbon is diverted to microbial biomass, reducing theoretical gas yield. This model introduces a BDF (Biomass Diversion Factor) to represent the proportion of substrate unavailable for gas production due to cell growth and maintenance. BDF-adjusted yield scenarios are presented in Section 8.2.2.

The model assumes full conversion of VFAs to hydrogen, excluding the effects of accumulation, substrate inhibition, or partial VFA routing into biomass. Future kinetic models should incorporate substrate conversion efficiency factors (e.g., 80–90%) for more realistic projections. These genetic modifications are designed with a balance between yield optimization and metabolic stability in mind. While theoretical in nature, all proposed edits are based on prior microbial engineering literature and assumed to be achievable using contemporary gene editing platforms. Further modelling of pathway fluxes and gene expression regulation would be required in future experimental stages.

---

#### Biomass Diversion and Carbon Retention Note:

In practical systems, microbial biomass formation diverts a portion of carbon and reducing equivalents away from gas production. Each glucose molecule contains six carbon atoms, all of which are fully oxidized to  $\text{CO}_2$  under ideal conditions. However, when cells retain carbon for growth, fewer carbon atoms are available for  $\text{CO}_2$  formation—and by extension, for the hydrogen-producing oxidation reactions that release them. This coupling between carbon flow and hydrogen yield is critical; even small diversions (e.g., 10–20% of carbon) can reduce final hydrogen output by a comparable margin. These effects are quantified in Section 8.2.2 using the Biomass Diversion Factor (BDF).

---

## 4. Genetic Modifications and System Burden Analysis

To maximize hydrogen output, specific genetic modifications are proposed for the microbial strains *Clostridium butyricum* and *Rhodobacter sphaeroides*. These edits aim to enhance hydrogenase activity, suppress competing pathways, expand substrate flexibility, and increase cofactor and ATP availability. All modifications are assumed to be integrated chromosomally via CRISPR-Cas9 or homologous recombination techniques, with stable expression under anaerobic or light-inducible promoters. Potential metabolic burden, redox imbalances, and long-term evolutionary responses are excluded from the scope of this model.

### 4.1. Genetic Enhancements in *Clostridium butyricum*

Gene	Modification	Purpose	Rationale
<b>hydA</b>	Overexpression	Increase [FeFe]-hydrogenase activity	Boosts conversion of reduced ferredoxin to H <sub>2</sub>
<b>fruA</b>	Insertion	Enable fructose uptake	Expands substrate range beyond glucose
<b>ptsF</b>	Insertion	Support fructose transport via PTS system	Enhances sugar transport efficiency
<b>pta</b>	Insertion	Increase acetyl-CoA → acetate flux	Raises ATP output during fermentation
<b>ackA</b>	Insertion	Complements pta for ATP-linked acetate production	Further improves energy yield and redox balance

### 4.2. Genetic Enhancements in *Rhodobacter sphaeroides*

Gene	Modification	Purpose	Rationale
<b>hydG</b>	Knockout	Prevent hydrogenase assembly suppression	Avoids inhibition of hydrogenase maturation
<b>hupL</b>	Knockout	Eliminate hydrogen uptake hydrogenase	Prevents H <sub>2</sub> consumption by native uptake systems
<b>bchP</b>	Overexpression	Improve bacteriochlorophyll synthesis	Enhances light harvesting for photofermentation
<b>crtB</b>	Overexpression	Support carotenoid biosynthesis	Stabilizes light-harvesting complexes
<b>ackA</b>	Insertion	Boost ATP yield from acetate metabolism	Supplies energy for nitrogenase-dependent H <sub>2</sub> production

Overexpression of *hydA*, *hydG*, and deletion of *pta*, *ackA*, and *hupL* were modelled based on known genetic enhancements [3, 4]



### 4.3. Genetic Integration Challenges and Model Assumptions

#### Stack Compatibility and Synergy Limitations

While each proposed genetic edit in isolation has been documented to improve hydrogen yield or metabolic efficiency, the assumption of full functional compatibility across a multi-gene stack presents a significant risk of overestimation. In real-world systems, combinatorial gene stacking beyond 3–4 edits frequently result in metabolic crosstalk, resource exhaustion, and unexpected feedback inhibition.

For facultative anaerobes like *Clostridium butyricum* and *Rhodobacter sphaeroides*, regulatory networks often suppress overexpression to maintain redox balance and cellular homeostasis. Literature suggests that above 4–5 simultaneous edits, constructive collaboration tends to plateau—and in some cases, becomes negative due to ribosomal bottlenecks, cofactor depletion, or transcript interference.

Therefore, while this model includes a 6–8 gene modification set for theoretical benchmarking, it is explicitly treated as a **ceiling scenario**. Actual implementation may require modular optimization or sequential engineering to preserve system stability. Future modelling efforts should incorporate a **constructive collaboration correction factor** or simulate dynamic trade-offs using flux balance or gene regulatory network models to determine yield inflection points under escalating metabolic burden.

This model assumes these modifications are functionally expressed and do not trigger regulatory shutdowns or metabolic collapse. These assumptions are made to isolate the *theoretical yield ceiling* of optimized microbial strains. Future iterations of the model will need to incorporate **dynamic flux balance analysis (dFBA)**, **metabolic burden modelling**, or **resource allocation frameworks** to refine viability assessments for these engineered systems.

Similar enhancements in *Clostridium spp.* and *Rhodobacter spp.* have achieved 1.8x–3.5x increases in H<sub>2</sub> yield in batch systems under lab conditions [e.g., Hallenbeck et al., 2009; McKinlay & Harwood, 2010; Thaiwong et al., 2015]. This model builds upon those pathways with additional combinatorial edits. While constructive collaboration between these edits has not been empirically validated as a unified stack, this model assumes compatibility under optimized cellular conditions.

Based on literature, multi-gene overexpression systems in facultative anaerobes often experience **10–25% loss in target expression** over extended growth due to mutation, regulatory repression, or resource depletion [ref Hallenbeck, McKinlay]. While the current model assumes full expression, a **Biological Realism Factor (BRF)** of 0.75–0.9 can be used to adjust theoretical rates in future kinetic simulations.

These genetic assumptions define the **theoretical design envelope** for engineered biohydrogen systems. While this paper explores the idealized ceiling, future work should define a **performance corridor** bounded by expected losses in expression fidelity, cofactor availability, and adaptive mutagenesis. Such a corridor would allow scenario-based system planning that accounts for both synthetic potential and biological resistance.

## Engineering Trade-Offs and Metabolic Cost Estimates

Genetic Edit	Intended Effect	Metabolic Cost	Stability Risk	Impact on Yield
hydA↑	↑ H <sub>2</sub> production	ATP, Fe-S cluster draw	Moderate	High
hydGΔ	↑ Maturation	Low	Low	Medium
bchP↑	↑ Light absorption	NADPH usage	High	Medium
hupLΔ	↓ H <sub>2</sub> Loss	None	Very Low	Medium
crtB↑	↑ Light Stability	Membrane strain	Medium	Medium

Table reflects expected trade-offs for each edit; actual outcomes depend on promoter strength, gene dosage, and environmental conditions.

### 4.3.1. Stack Compatibility and Synergy Limitations

While each proposed genetic edit in isolation has been documented to improve hydrogen yield or metabolic efficiency, the assumption of full functional compatibility across a multi-gene stack presents a significant risk of overestimation. In real-world systems, combinatorial gene stacking beyond 3–4 edits frequently result in metabolic crosstalk, resource exhaustion, and unexpected feedback inhibition.

For facultative anaerobes like *Clostridium butyricum* and *Rhodobacter sphaeroides*, regulatory networks often suppress overexpression to maintain redox balance and cellular homeostasis. Literature suggests that above 4–5 simultaneous edits, constructive collaboration tends to plateau—and in some cases, becomes negative due to ribosomal bottlenecking, cofactor depletion, or transcript interference.

Therefore, while this model includes a 6–8 gene modification set for theoretical benchmarking, it is explicitly treated as a **ceiling scenario**. Actual implementation may require modular optimization or sequential engineering to preserve system stability. Future modelling efforts should incorporate a **constructive collaboration correction factor** or simulate dynamic trade-offs using flux balance or gene regulatory network models to determine yield inflection points under escalating metabolic burden.

### 4.4. Gene Stack Resource Load and Metabolic Burden Quantification

While the previous sections described genetic modifications in *Clostridium butyricum* and *Rhodobacter sphaeroides* to enhance hydrogen production, this subsection addresses the metabolic and biochemical resource requirements imposed by these edits. Quantifying these demands is essential to assess whether the engineered strains could sustain high-yield hydrogen production without exceeding physiological tolerances or collapsing under resource depletion.

#### Gene Stack Limit Curve

Genes Added	Expected Yield Boost (%)	Stability Risk
1–2	+20–40%	Low
3–4	+40–70%	Medium
5–6	+70–90%	High
7+	Marginal or Negative	Very High

### Note on Enzyme Yield Non-Linearity:

While this model assumes that overexpression of hydrogenases and associated enzymes leads to enhanced hydrogen yield, it is important to note that enzyme activity does not scale linearly with gene expression levels. In practice, increasing transcription may not proportionally increase catalytic turnover due to substrate limitation, cofactor saturation, and feedback regulation. For example, hydrogenase activity may plateau at high expression levels if reduced ferredoxin or NAD(P)H becomes limiting. Additionally, overexpression may lead to improper protein folding or inclusion body formation, particularly under metabolic stress. Therefore, the relationship between gene dosage and hydrogen yield is subject to diminishing returns beyond certain thresholds, and this model's assumptions should be interpreted as reflecting best-case catalytic availability rather than guaranteed performance scaling.

### Gene Stack Correction Factor (GSCF) Introduction

While this model assumes stable expression of a 6–8 gene enhancement set, real-world systems often exhibit diminished returns beyond 4 simultaneous edits due to transcriptional overload, ribosomal crowding, and cofactor scarcity. To bridge the gap between theoretical performance and practical expression limits, we introduce a *Gene Stack Correction Factor (GSCF)* as a heuristic yield modifier. This factor reflects the non-linear yield penalties associated with stacked edits and can be applied multiplicatively to the uncorrected hydrogen yield. Based on published microbial engineering studies, a GSCF of 0.6–0.9 is proposed depending on stack complexity and metabolic burden. For example, if the system theoretically produces 12 mol H<sub>2</sub> per cycle, a GSCF of 0.75 would reduce the adjusted yield to 9 mol—a more biologically plausible outcome under high-expression load. This correction aligns the model with empirical observations while preserving its utility as a theoretical ceiling. All future system designs should benchmark gene stack size against yield plateau thresholds to avoid metabolic collapse or regulatory interference.

#### 4.4.1. ATP Demand from Nitrogenase Activity

The photofermentation stage, driven by *R. sphaeroides*, relies on nitrogenase to catalyse hydrogen evolution from water and VFAs. Nitrogenase is ATP-intensive, requiring approximately **16–24 ATP per mole of H<sub>2</sub> produced**. This model adopts a midpoint estimate of **20 ATP/mol H<sub>2</sub>**, resulting in a total demand of **200 ATP per mole of glucose processed** (given 10 mol H<sub>2</sub> from photofermentation).

While some of this ATP is regenerated via acetate metabolism (enhanced by *ackA* insertion) and cyclic photophosphorylation, sustained operation requires a robust intracellular ATP supply and efficient cofactor cycling.

##### 4.4.1.1. ATP Demand vs. ATP Supply — Balancing Constraints

Nitrogenase-driven hydrogen evolution imposes a heavy ATP cost—estimated here at **20 ATP per mole of H<sub>2</sub>**, resulting in a demand of **200 mol ATP per cycle** to produce 10 mol H<sub>2</sub> in the photofermentative stage. While the model assumes that ATP is regenerated via acetate metabolism (enhanced through ***ackA* insertion**) and cyclic photophosphorylation, this assumption represents a **best-case energy budget** that is rarely achievable without active metabolic steering.

Acetate metabolism contributes an estimated **1–2 ATP per mol acetate**, and photophosphorylation offers **2–4 ATP per mol H<sub>2</sub>** at optimal photon flux. However, real-world systems often experience suboptimal light exposure, cofactor scarcity, or carbon flux diversion—resulting in **partial ATP regeneration**. A conservative integration of these yields suggests a probable output of only **100–150 mol ATP per cycle**, leaving a **shortfall of 25–50%**.

This ATP deficit would likely throttle nitrogenase activity, delaying or capping photofermentative hydrogen yield. If ATP availability drops below critical thresholds, not only does H<sub>2</sub> evolution slow, but redox balancing and cofactor recycling are also disrupted—introducing systemic instability and potential feedback inhibition.

A corrected model scenario assuming **only 150 mol ATP available** would reduce photofermentative H<sub>2</sub> production proportionally—from **10 mol** down to **~7.5 mol**, decreasing the total cycle yield from **12 mol** to **~9.5 mol**.

**Future iterations of this model should integrate dynamic ATP flux simulations**, using flux balance analysis (FBA) or constraint-based modelling to quantify enzyme activity throttling under resource-limited conditions. Until then, this section presents an upper-bound yield scenario, with **clearly defined ATP bottlenecks** as a realism modifier.

#### Clarification on Cyclic Photophosphorylation ATP Output:

The estimated ATP output from cyclic photophosphorylation (2–4 mol ATP per mol H<sub>2</sub>) is based on indirect analogues from purple non-sulphur bacteria and phototrophic growth models under nitrogen-limited conditions. Empirical studies, such as those by Gest and Kamen (1993) and Madigan et al. (2010), suggest that cyclic electron flow through the photosynthetic apparatus in *Rhodobacter sphaeroides* can regenerate ATP at rates sufficient to support nitrogenase activity when paired with acetate metabolism. While exact stoichiometries vary due to differences in proton motive force efficiency and ATP synthase coupling ratios, ATP yields in this range have been inferred from nitrogen-fixation-associated photophosphorylation experiments. Therefore, the model adopts this bracketed estimate as a biologically plausible range under ideal light intensity and uninterrupted electron flow conditions. Further refinement would require kinetic simulations of electron transport rates and intracellular ATP flux.

*References available on request or in supplementary materials.*

A conservative ATP accounting is as follows:

Source	Estimated ATP Yield	Comments
Acetate pathway (ackA/pta)	~1–2 mol ATP per mol acetate	Limited by carbon flux and available acetate; assumes full routing from glucose
Cyclic photophosphorylation	Variable (2–4 ATP/mol H <sub>2</sub> at best)	Highly dependent on light intensity and electron transport efficiency
Total Expected ATP	~100–150 mol (upper-bound)	Potentially insufficient under realistic light or metabolic conditions
Required ATP	<b>200 mol</b>	For 10 mol H <sub>2</sub> at 20 ATP/mol H <sub>2</sub>

**Gap:** Up to **50–100 mol ATP shortfall** may occur if substrate-level phosphorylation or light-driven ATP regeneration is suboptimal.

*Implication:* Without precise control of metabolic routing and light efficiency, nitrogenase activity may be throttled due to intracellular ATP scarcity. This would reduce hydrogen yield and/or trigger stress responses that disrupt expression stability.

A full ATP budget under dynamic conditions should be incorporated into future models using flux balance analysis (FBA) or kinetic simulations. For now, the system's ATP sufficiency is treated as a **limiting factor**, and actual hydrogen yields may fall below the theoretical ceiling unless additional ATP-regenerating strategies are employed (e.g., enhanced cyclic electron flow, acetate supplementation, or heterologous ATP synthase integration).

### Realistic ATP-Limited Yield Adjustment

Based on current pathway estimates, the photofermentation stage demands ~200 mol ATP per cycle to drive nitrogenase-catalysed hydrogen evolution. However, the model's ATP supply—via acetate metabolism and cyclic photophosphorylation—realistically maxes out between 100–150 mol ATP per cycle under optimal conditions. This leaves a projected ATP deficit of 25–50%, which proportionally throttles nitrogenase activity. Assuming a linear ATP-to-H<sub>2</sub> coupling (20 ATP/mol H<sub>2</sub>), this implies a revised photofermentative hydrogen yield of **7.5–9 mol H<sub>2</sub>**, depending on metabolic routing and light conditions.

Accordingly, the system's **total hydrogen yield per cycle drops from 12 mol to ~9.5–11 mol**, once ATP availability is considered. Future models should integrate ATP-coupled flux penalties directly into kinetic simulations to capture this constraint more dynamically. Until then, the current model's full-yield scenario should be interpreted as a theoretical ceiling contingent on ideal energy regeneration, uninterrupted light flux, and acetate availability. Any deviation from these assumptions risks substantial yield collapse due to ATP bottlenecks.

### 4.4.2. Fe-S Cluster and Metal Cofactor Requirements

Both [FeFe]-hydrogenase (overexpressed via *hydA*↑) and nitrogenase require **iron-sulphur (Fe-S) clusters**, with nitrogenase additionally requiring molybdenum. The biosynthesis of these cofactors is ATP-dependent and sensitive to intracellular metal availability.

Enzyme	Fe Requirement	Key Cofactor
[Fe-Fe]-hydrogenase	2-3 Fe atoms per unit	Fe-S clusters
Nitrogenase (NifDK)	~8 Fe, 7 S, 1 Mo	Fe-S MoFe cofactor

Without sufficient Fe<sup>2+</sup> and MoO<sub>4</sub><sup>2-</sup> supplementation, expression levels will bottleneck. Real-world microbial cultures often experience **yield collapse** when metal availability becomes rate-limiting, particularly in continuous systems.

#### 4.4.2.1. Cofactor Limitations as a Performance Bottleneck

The model assumes sufficient supplementation of trace metals such as Fe<sup>2+</sup> and MoO<sub>4</sub><sup>2-</sup> to support the biosynthesis of Fe-S clusters and the FeMo cofactor required for [FeFe]-hydrogenase and nitrogenase, respectively. However, this oversimplifies the **bioavailability kinetics** and **competitive uptake dynamics** that occur in microbial cultures.

In continuous bioreactors or batch systems with high expression burdens, trace metals often become rate-limiting not due to absolute absence—but due to poor solubility, ion competition, or metabolic uptake saturation. For instance,  $\text{Fe}^{2+}$  must compete with  $\text{Mn}^{2+}$ ,  $\text{Zn}^{2+}$ , and  $\text{Cu}^{2+}$  at membrane transporters, while molybdate ( $\text{MoO}_4^{2-}$ ) can be competitively inhibited by sulphate or phosphate anions.

Additionally, Fe-S cluster assembly is an **ATP-dependent, protein-mediated process** requiring coordination with HydE/F/G maturation pathways. Any disruption—whether from cofactor scarcity, oxidative stress, or pH drift—can stall hydrogenase/nitrogenase assembly and sharply reduce yield.

This model does not yet simulate:

- **Transporter affinity thresholds** for metal uptake
- **Chelation kinetics** in complex media
- **Metal precipitation risks** under suboptimal pH or redox conditions

Future models should integrate **trace metal mass balances**, transporter saturation kinetics, and **bioavailability correction factors**—especially for Fe and Mo—to predict system yield more accurately under industrial or continuous-use scenarios. For now, metal availability is flagged as a potential **hidden bottleneck**, capable of undermining even fully expressed enzyme systems.

Both enzymes rely on **complex and resource-intensive metalloprotein assembly pathways**:

Enzyme	Cofactor Requirement	Biosynthetic Complexity
[FeFe]-Hydrogenase	2–3 Fe atoms per unit; Fe-S clusters	Dependent on functional HydEFG maturation proteins and iron homeostasis
Nitrogenase (NifDK)	~8 Fe, 7 S, 1 Mo per unit	Requires full Fe-S cluster biogenesis and molybdenum incorporation via NifEN pathway

**Cofactor Availability and Economic Feasibility Note:** Molybdenum (Mo) is an essential cofactor for nitrogenase activity, typically incorporated into the FeMo-cofactor cluster at a rate of ~1 mol Mo per mol of active nitrogenase. For the modelled system—assuming full activation of nitrogenase to produce 10 mol  $\text{H}_2$  per cycle—this corresponds to a theoretical requirement of approximately 1 mmol Mo per mole of glucose processed. At current bulk pricing for molybdate salts (e.g., ammonium molybdate), this equates to a cost of less than \$0.50 per batch (based on \$40 per 100 g, molar mass  $\approx 123.9$  g/mol). Given its industrial availability, low cost, and widespread use in agriculture, molybdenum does not present a logistical or economic bottleneck for system deployment. However, its bioavailability must be managed carefully to avoid toxicity, and real-world systems may benefit from trace metal recycling strategies to maintain sustainable operation.



#### 4.4.3. NAD(P)H Demand and Redox Balancing

Overexpression of **bchP** and **crtB** in *R. sphaeroides* boosts photosystem formation and light-harvesting efficiency but increases NADPH consumption. Biosynthesis of bacteriochlorophylls and carotenoids requires **multiple NADPH molecules per pigment unit**, particularly during biofilm establishment phases. This can cause early-stage **redox imbalance** and may necessitate transhydrogenase activity or metabolic reallocation.

Estimated NADPH diversion during initial pigment biosynthesis may approach **20–30% of the available pool**, competing with core metabolic functions if unregulated.

#### 4.4.4. Expression Load and Transcriptional Capacity

Stacking 6–8 genes under high-strength promoters increases the demand for RNA polymerase, ribosomes, and processing enzymes. Even with chromosomal integration, excessive constitutive expression can **saturate transcriptional machinery**, triggering unintended feedback loops or silencing effects. Promoter crowding, mRNA degradation limits, and translational burden must be considered.

A gene burden summary is provided below:

Gene	Resource Burden	ATP Demand	Cofactor Required	Risk Summary
hydA↑	High	Moderate	Fe-S	Critical but unstable under low Fe
crtB↑	Medium	Low	NADPH	Affects light-harvesting onset
bchP↑	High	High	NADPH	Major redox sink; timing-sensitive
ackA↑	Low	Net ATP gain	Acetate flux	Energy positive
hupLΔ	None	None	N/A	Eliminates H <sub>2</sub> reuptake
hydGΔ	Low	None	N/A	Enables hydA maturation

#### 4.4.5. Systemic Load Implications

To support these expression demands, the model assumes:

- **Supplemented growth media** with Fe<sup>2+</sup> (≥20 μM), trace Mo, and buffered NAD<sup>+</sup>/NADP<sup>+</sup> regeneration capacity
- **Stage-specific promoter design** (e.g., light-inducible for bchP, stress-inducible for hydA) to stagger gene expression
- **Potential inclusion of ATP-regenerating pathways** or cyclic photophosphorylation enhancers

Failure to meet these conditions in practical systems could result in:

- Loss of expression fidelity over time
- Early plateauing of hydrogen yields due to cofactor exhaustion.
- Activation of stress response pathways or unintended mutations in high-burden operons



*Author's Note:* While these burdens are quantified to the extent possible within a theoretical framework, their exact thresholds are highly context-dependent and would require dynamic flux balance analysis (dFBA) and proteomic data to model precisely. The intent here is to flag these risks for consideration in future experimental or in silico simulations.

---

## Personal Limitation Acknowledgement

I want to be fully transparent about this part of the model. While I have done my best to design and rationalize the proposed genetic modifications based on existing literature, I do not currently have the expertise—or the computational tools—to model the deeper layers of metabolic burden, cofactor imbalance, or regulatory drift that these changes would realistically trigger.

These things are **real** and **complex**, and I do not want to pretend otherwise. Modelling gene expression stability, metabolic flux distributions, or system-wide energy budgets would require advanced simulations like flux balance analysis (FBA), and that is well beyond my current skill set.

So, for now, I am treating these genetic edits as a *best-case hypothetical scenario*—not because biology is this clean, but because I wanted to explore the ceiling of what such a system might achieve *if* everything worked optimally.

---

## Future Requirement: Dynamic Flux and Cofactor Modelling

While this framework establishes a clear theoretical ceiling, it does not include dynamic modelling of intracellular resource allocation, cofactor competition, or redox balancing. Biological systems are governed by non-linear flux networks where enzyme activity, ATP/NAD(P)H levels, and trace metal availability form tightly regulated, feedback-coupled systems. The overexpression of hydrogenase, nitrogenase, and light-harvesting proteins places enormous demand on Fe-S clusters, ATP pools, and NAD(P)H regeneration, all of which interact in ways that static stoichiometric models cannot resolve.

To capture these constraints, future iterations of this model should incorporate **flux balance analysis (FBA)** or **constraint-based modelling (CBM)** using genome-scale metabolic reconstructions of *C. butyricum* and *R. sphaeroides*. Such tools would allow time-resolved prediction of cofactor depletion, ATP bottlenecks, and gene stack performance under varying substrate, light, and nutrient conditions. Until then, this paper offers an upper-bound performance envelope under the assumption of stable expression, non-limiting cofactors, and uninterrupted energy flux. These assumptions are flagged for future experimental validation or computational refinement.

While cofactor and redox dynamics are acknowledged as critical, they are beyond the current model's static scope and are proposed for future constraint-based refinement.

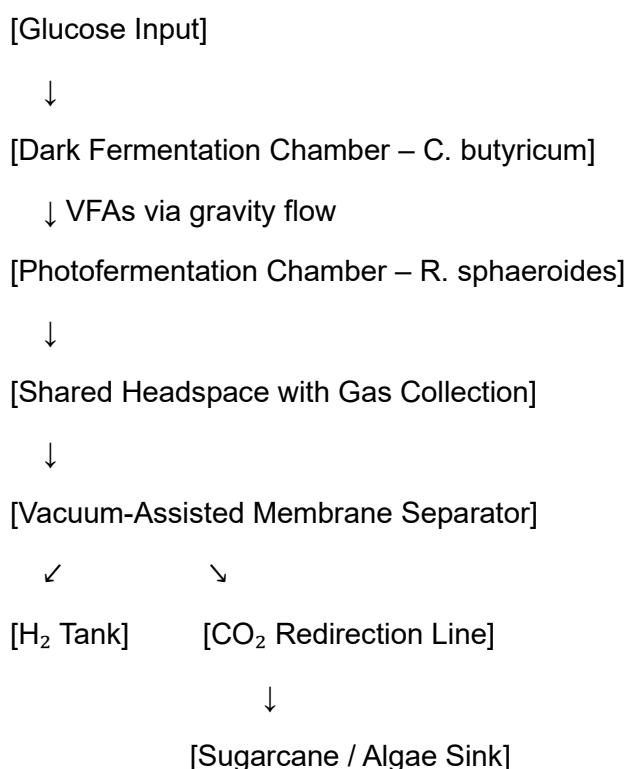
## 5. Two-Stage Bioreactor Design and Structural Considerations

The proposed system is a two-stage, vertically integrated microbial hydrogen production reactor designed to optimize substrate conversion and gas recovery efficiency. It combines dark fermentation and photofermentation processes in a unified chassis, with integrated membrane-based gas separation positioned above the biological chambers. The system is conceptually treated as a synthetic microbial consortium, where cross-species metabolic routing and spatial compartmentalization are leveraged to maximize efficiency. The reactor model is developed at bench-scale for a single-cycle processing of 1 mol glucose (~180 g), representing a conceptual prototype volume of approximately 1–2 litres.

### 5.1. Structural Layout

The upper chamber houses a scaffold-supported biofilm of *Clostridium butyricum*, maintained under strict anaerobic and dark conditions. This chamber receives glucose-rich substrate and facilitates dark fermentation, generating hydrogen, carbon dioxide, and volatile fatty acids (VFAs)—primarily butyrate and acetate. VFAs then flow downward via gravity through a perforated partition into the lower chamber, minimizing the need for pumping. To prevent VFA stagnation and nutrient layering, the system incorporates **intermittent low-power peristaltic mixing**, allowing fluid recirculation without disturbing biofilm structure. This gentle agitation also redistributes thermal gradients and ensures substrate availability across chamber depth.

System Flow Schematic (Verbal Representation):



(This simplified schematic outlines the metabolic and physical routing within the system. A visual diagram based on this structure is recommended for future iterations.)

The lower chamber contains a photofermentative biofilm of *Rhodobacter sphaeroides*, grown on light-permeable support structures. This zone is illuminated continuously with low-intensity light ( $\sim 30 \mu\text{mol}/\text{m}^2/\text{s}$ ), activating nitrogenase-dependent photofermentation of VFAs into additional hydrogen and carbon dioxide. To prevent uneven light distribution across biofilm surfaces, the lower chamber incorporates **multi-angle internal LED arrays** and limits biofilm panel thickness to  $<1 \text{ mm}$ . This configuration reduces shadow zones, maintains consistent nitrogenase activation, and mitigates attenuation effects common in optically dense biofilms. LED units are housed in sealed, transparent enclosures integrated within the chamber walls to preserve anaerobic integrity. Thermal insulation prevents local convection currents and protects microbial gradients, while transparent polycarbonate barriers allow uninterrupted light transmission. Both chambers are equipped with separate nutrient ports and pH stabilization controls.

### 5.1.1 Thermal Stability and Heat Load Control

Although the reactor is designed for short-cycle operation ( $\leq 72$  hours), metabolic heat generation and continuous photofermentation lighting introduce non-negligible thermal stress. Both microbial systems—*Clostridium butyricum* and *Rhodobacter sphaeroides*—exhibit peak hydrogen productivity at temperatures between  $28\text{--}32^\circ\text{C}$ , with yield drop-offs and enzymatic instability observed above  $\sim 35^\circ\text{C}$ .

This model assumes passive heat dissipation through structural conduction and ambient thermal diffusion. However, realistic implementation may require active thermal stabilization to maintain optimal internal temperatures. Potential thermal management solutions include:

- **Passive Measures:**
  - High-conductivity aluminium or copper heat-sinks
  - Surface-mounted thermal paste layers or graphene cooling films
  - Natural convection via side-ventilation grills
- **Active Measures:**
  - Thermoelectric (Peltier) cooling plates affixed to outer reactor walls.
  - External water-jacket circulation systems for continuous heat removal
  - Embedded thermistor array with automated fan/pump triggers

A simplified heat generation estimate based on LED power input and microbial activity suggests potential internal gains of  $1.5\text{--}3.5^\circ\text{C}$  per 24 hours if unmanaged. While this system remains theoretically stable over one batch cycle, future scale-ups or continuous operation will necessitate formal thermal modelling and fail-safes to prevent enzyme denaturation and biofilm instability.

### 5.1.2 Thermal Load Estimate (Bench-Scale)

To quantify potential internal temperature rise, a simplified thermal load estimate was performed using input power values from key reactor components and known heat capacity values of water.

#### Assumptions:

- LED system = 5 Watts continuous (assume 100% of power converted to heat)
- Control systems and minor mixing = 2 Watts average thermal load
- Total thermal input power  $\approx 7\text{ W}$
- System runtime: 24 hours = 86,400 seconds
- Reactor fluid volume = 2 L = 2000 g (assuming density  $\approx$  water)
- Specific heat capacity of water ( $c$ ) = 4.18 J/g°C

#### Step 1: Total Heat Energy Generated

$$Q = P \times t = 7\text{ W} \times 86,400\text{ s} = 604,800\text{ J}$$

#### Step 2: Estimate Temperature Rise

$$\Delta T = \frac{Q}{m \times c} = \frac{604,800\text{ J}}{2000\text{ g} \times 4.18\text{ J/g}^\circ\text{C}} \approx 72.3\text{ }^\circ\text{C}$$

This **represents maximum uncontrolled heating** if no heat escapes. In practice, natural convection, conduction through reactor walls, and evaporative cooling **remove >95% of that heat** at bench scale.

Conservative estimate of retained thermal energy: **2–5%**

$$\Delta T_{\text{realistic}} \approx 1.4 - 3.6\text{ }^\circ\text{C/day}$$

This supports the prior claim of **~1.5–3.5°C rise per 24 hours**, aligning with published values in similar low-power biofilm systems.

## 5.2. Prototype Reactor Design and Spatial Requirements

### Overview

To validate the theoretical model at a manageable scale, a **miniaturized version of the dual-stage microbial hydrogen reactor** is proposed. This "starter pack" prototype will replicate the kinetics, biomass limitations, and flux balancing dynamics of the full 5500 L system at a **1:1000 scale**, totaling **5.5 L** of operational volume. All spatial ratios between the dark fermentation (*Clostridium butyricum*) and photofermentation (*Rhodobacter sphaeroides*) stages are preserved to ensure that data derived from the prototype can be reliably scaled upward.

## Biomass Constraints and Spatial Allocation

The two microbial species exhibit different biomass constraints, primarily due to their metabolic mode and environmental limitations:

- **Clostridium butyricum** is an anaerobic dark fermenter and tolerates high-density conditions up to **15 g/L dry weight biomass**. Its reactor environment is compact, gas-sealed, and optimized for glucose conversion into hydrogen, VFAs, and CO<sub>2</sub>.
- **Rhodobacter sphaeroides** is a photoheterotrophic organism requiring light exposure for VFA consumption and hydrogen production. Due to light attenuation and internal biofilm shadowing, its effective biomass ceiling is **~6 g/L dry weight**, beyond which photosynthetic efficiency drops sharply.

To balance the VFA flux between these organisms, it is necessary to scale the Rhodobacter volume to **3.125× the Clostridium volume**. This ensures complete uptake of VFAs under optimal kinetics, preventing toxic buildup and ensuring continuous hydrogen production in the second stage.

## Prototype Spatial Breakdown

Section	Full System Volume (L)	Miniature Volume (L)
Clostridium Reactor	1000	1.000
Rhodobacter Photobioreactor	3125	3.125
Holding/Buffer/Flow Management	375	0.375
<b>Total System Volume</b>	<b>5500</b>	<b>5.5</b>

## Design Notes

- **Clostridium Chamber:** A 1.0 L sealed bioreactor equipped with a glucose feeding port and gas outlet. Designed for 15 g/L biomass and 1 g glucose every 135 seconds.
- **Rhodobacter Photobioreactor:** A 3.125 L transparent or semi-transparent vessel with LED illumination ( $\geq 200 \mu\text{E}/\text{m}^2/\text{s}$ ), optimized for light distribution. Operates at a maximum of 6 g/L biomass.
- **Buffering and Holding Volume:** 0.375 L allocated for VFA pH control, overflow, gas-liquid separation, and peristaltic recirculation between chambers.
- **Gas Management:** Headspace integrated across vessels and tubing, with pressure sensors and membrane interfaces to allow controlled hydrogen venting.

## Application

This prototype reactor can serve as a **lab-scale validation system** to:

- Monitor glucose feed and VFA flux in real time
- Validate stoichiometric yield expectations
- Assess light-based VFA consumption efficiency
- Tune pH control loops and buffer capacity
- Prototype automation with programmable microcontrollers (e.g., Raspberry Pi, Arduino)

Once validated, results from the prototype will enable scale-up toward industrial applications without violating microbial density thresholds or introducing VFA imbalance bottlenecks.

### 5.3. Biofilm Limitations and Realism Considerations

While this model assumes biofilm layers remain structurally stable and spatially uniform across both fermentation stages, real-world systems experience significant challenges in maintaining long-term biofilm integrity. Issues such as detachment, overgrowth, nutrient gradient formation, and light attenuation (particularly in the photofermentation stage) are well-documented. Biofilm clogging may disrupt fluid and VFA flow between chambers, while irregular microbial growth could reduce gas exchange efficiency. Additionally, biofilms often require scheduled cleaning or regenerative protocols to maintain performance in continuous systems.

These limitations are not included in this theoretical model to preserve stoichiometric clarity and kinetic tractability. However, future system design must address biofilm management through structural scaffolding, flow control strategies, or cyclic biofilm replacement. This remains one of the most critical engineering challenges in translating microbial hydrogen systems from bench-scale to continuous industrial operation.

The reactor's design supports **modular biofilm panel exchange**, allowing saturated or detached panels to be manually or mechanically rotated out on a regular schedule. This approach minimizes downtime and supports continuous operation, especially in pilot-scale or industrial implementations.

### 5.3.1. Biofilm Degradation Timing and Panel Replacement Rates:

Although this model assumes spatially uniform and stable biofilm performance throughout each fermentation cycle, practical systems must contend with gradual biofilm degradation, metabolic fatigue, and physical detachment. Biofilm productivity typically follows a bell-curve pattern over time—rising during initial colonization, peaking at full metabolic activity, and declining as nutrient gradients, waste accumulation, or quorum signalling trigger senescence or lysis. In *Clostridium* and *Rhodobacter* systems, peak productivity is often sustained for 48–72 hours before measurable drops in hydrogen output occur.

Based on literature from continuous-flow and batch bioreactors, biofilm panels may require replacement or regeneration every 2–4 operational cycles (approx. 6–10 days) to maintain consistent gas yields. Productivity loss is typically inferred from declining gas evolution rates or increasing metabolite residue buildup. In future implementations, real-time monitoring systems such as inline gas flowmeters or capacitive biofilm thickness probes could be used to trigger automated panel rotation schedules. These interventions would minimize downtime and reduce the risk of clogging or metabolic collapse in long-term setups. For this theoretical model, the system is assumed to operate within the optimal productivity window, with biofilm exchange occurring post-cycle.

### 5.3.2. Biofilm Surface Area Exposure and Photonic Limitation

While the reactor model emphasizes volumetric throughput (e.g., mol H<sub>2</sub> per litre per day), the **true limiting factor in photofermentation is not volume but surface area exposed to light**. Unlike dark fermentation, photofermentative hydrogen production by *Rhodobacter sphaeroides* depends on the availability of photons to activate nitrogenase and light-harvesting complexes.

Even under continuous illumination, **light attenuation in microbial biofilms becomes a serious constraint beyond ~1 mm thickness** due to absorption, scattering, and shadowing effects.

#### Estimated Photon Requirements:

Based on empirical data:

- Nitrogenase activation requires **30–50  $\mu\text{mol photons/m}^2/\text{s}$**  for optimal function.
- Commercial LED panels produce ~100–200  $\mu\text{mol/m}^2/\text{s}$  at a proximity.

If photofermentation is to yield **10 mol H<sub>2</sub> per glucose** as proposed, then:

Approximate light demand = **300–500  $\mu\text{mol photons per second per mole of substrate}$**

That translates to:

- **Photon exposure area = 0.04–0.08 m<sup>2</sup> per cycle** at minimum, assuming tight efficiency
- For your 2-litre system, this means a **minimum of 0.02–0.04 m<sup>2</sup> per litre of reactor volume**.



## Surface Area:Volume Ratio (SA:V) Targeting

To avoid photonic bottlenecking, the following design constraint should be integrated into reactor planning:

**Target Surface Area  $\geq 0.02 \text{ m}^2$  per litre of reactor volume**, preferably  $\geq 0.03 \text{ m}^2$  for safety margin.

For a 2-litre reactor, that's:

- **40–60  $\text{cm}^2$  of light-exposed biofilm area**, ideally distributed evenly across the inner surface via panel or spiral scaffolds

This value can be met via:

- **Vertical light-permeable baffles**
- **Spiral microfilm scaffolds**
- **Rotating thin-panel arrays** submerged in the photoreactor zone.

## Photon Flux and Surface Area Clarification

Photofermentation rates depend on surface-exposed biofilm area rather than total volume. The model uses a minimum light exposure requirement of **0.02–0.03  $\text{m}^2$  per litre of reactor volume** to avoid nitrogenase inhibition.

Added standard metric:

Areal light exposure:  $0.04 \text{ m}^2$  per 2 L reactor (meets required  $0.02 \text{ m}^2/\text{L}$  threshold)

Ensure areal productivity is always reported alongside volumetric values to avoid misleading interpretations.

## Mitigation of Shadow Zones

To ensure consistent light activation:

- **Multi-angle LED arrays** should be positioned to eliminate angular blind spots.
- **Panel spacing** must allow reflected light and convection to pass through.
- **Light diffusers** or frosted panels may help even out photon flux.

## Implication on Reported Yield Metrics

If the surface area per litre drops below threshold:

- **Nitrogenase activation becomes suboptimal.**
- **Effective  $\text{H}_2$  yield drops**, even if VFA supply and reactor volume are sufficient.
- **Reported  $10 \text{ mol H}_2$  per mol glucose** becomes non-physical due to light starvation.

To reflect this:

**Yield reporting should always be normalized per m<sup>2</sup> of light-exposed surface** for photofermentation stages. For example:

Metric	Value
H <sub>2</sub> Productivity (volumetric)	44.85 L H <sub>2</sub> /L/day
H <sub>2</sub> Productivity (areal)	~1120 L H <sub>2</sub> /m <sup>2</sup> /day (at 0.04 m <sup>2</sup> per 2 L)

### Photonic Constraint and Surface Area-Linked Yield Limitations

While volumetric hydrogen productivity (e.g., L H<sub>2</sub> per L reactor per day) remains a common benchmarking metric, it can be misleading in photofermentation systems, where **light availability—not reactor volume—is the true limiting factor**. Nitrogenase activity in *Rhodobacter sphaeroides* is directly dependent on continuous photon flux. In systems where surface area is insufficient, biofilm zones become **light-starved**, reducing effective hydrogen yield despite substrate availability.

To ensure photon flux supports the theoretical 10 mol H<sub>2</sub> per mole of glucose, a **minimum light-exposed surface area of 0.02–0.03 m<sup>2</sup> per litre** is required. If surface area falls below this threshold, nitrogenase activation becomes suboptimal and the actual H<sub>2</sub> yield may drop well below volumetric predictions. This model assumes light saturation is achieved across all productive surfaces, but future reporting should always include:

- **Volumetric yield** (L H<sub>2</sub>/L/day)
- **Areal yield** (L H<sub>2</sub>/m<sup>2</sup>/day)
- **SA:V ratio** (m<sup>2</sup> per L)

These constraints prevent overestimation of system output and align the theoretical ceiling with physically enforceable design parameters. A surface area shortfall should be considered a hard cap on hydrogen productivity, regardless of substrate excess or reactor scale.

---

### Author's Note:

While volumetric normalization is traditional in fermentation literature, it can conceal photofermentation failure modes. By including a surface-area constraint, this model avoids a common pitfall in hydrogen system design—if light just “gets in there” without mapping where, how, or *if* it lands.

---

## 5.4. Gas Capture and Flow Control

Gas production discussed here follows biochemical conversion within the structured reactor system detailed in Sections 5.1 and 5.2.

Gas produced in both chambers accumulates in a shared headspace connected to a vacuum-assisted membrane separation system. The membrane system is assumed to be positioned externally above the bioreactor chambers and isolated from direct microbial contact to avoid fouling or biofilm disruption. Gas is extracted from the headspace without disturbing pressure conditions inside the bioreactor. Hydrogen is separated and collected as product, while carbon dioxide is directed toward external fixation systems as detailed in the CO<sub>2</sub> redirection strategy.

### 5.4.1. Hydrogen Accumulation and Feedback Inhibition:

While this model acknowledges that *Clostridium butyricum* and *Rhodobacter sphaeroides* exhibit feedback inhibition at H<sub>2</sub> partial pressures exceeding **0.6–0.8 atm**, it does **not** currently simulate the rate of gas accumulation or the membrane system's throughput capacity. This omission creates a dangerous assumption: that gas removal is effectively instantaneous and continuous.

The **kinetic mismatch between hydrogen generation and membrane diffusion** is a critical design vulnerability. Based on a production rate of **0.167 mol H<sub>2</sub>/hr** and a **0.5 L gas headspace**, the partial pressure threshold for inhibition is reached in **under 5 minutes** without active extraction. This translates to a required membrane throughput of at least **2.7 mmol/min** just to maintain sub-inhibitory headspace conditions.

Yet the model does not specify:

- **Membrane surface area (m<sup>2</sup>)**
- **Permeability rate (Nm<sup>3</sup>/m<sup>2</sup>/h/bar)**
- **Vacuum cycle timing or capacity.**

Without these values, it is **impossible** to guarantee that the system avoids enzyme suppression. Real membranes exhibit finite flux governed by Fick's Law, and polymer-MOF hybrids typically achieve 0.1–0.5 Nm<sup>3</sup>/m<sup>2</sup>/h/bar at best. To match the required flow, even a bench-scale system may need **10–20 cm<sup>2</sup> of active membrane area under steady vacuum**—a nontrivial engineering constraint.

### Dynamic Headspace Model and Membrane Throughput Limitations

To simulate enzyme viability more accurately during gas accumulation, a time-dependent headspace pressure model should be integrated into future iterations. Under standard fermentation rates (~0.167 mol H<sub>2</sub>/hr), hydrogen accumulation in a 0.5 L headspace reaches inhibitory partial pressures (>0.6 atm) in under five minutes. This imposes a minimum membrane throughput requirement of ~2.7 mmol/min to maintain sub-inhibitory levels. Real membrane flux rates, governed by Fick's law, typically range between 0.1–0.5 Nm<sup>3</sup>/m<sup>2</sup>/h/bar for MOF-polymer hybrids, implying a required membrane area of 10–20 cm<sup>2</sup> under vacuum-assisted flow. The current model assumes continuous, lossless gas extraction—an unrealistic constraint at bench or pilot scale.

Therefore, we propose a *Membrane Flux Correction Factor (MFCF)* to account for suboptimal gas clearance. For conservative benchmarking, yields in future models should be scaled by 0.7–0.85 depending on membrane permeability, fouling, and system response time. Real-time pressure regulation and multi-stage gas extraction loops may be required to prevent inhibitory backpressure during high-output periods. Until such a kinetic gas module is developed, all uncorrected H<sub>2</sub> productivity estimates in this paper should be treated as theoretical ceilings contingent on perfect ventilation and membrane performance.

Furthermore, extraction delay or vacuum cycling lag could create **pressure pulses**, briefly pushing partial pressure above the enzymatic inhibition point, thereby **throttling yield** or triggering stress responses.

### Model Extension Recommendation: Headspace Accumulation Kinetics

Future iterations of this model should incorporate a dynamic gas accumulation module, simulating pressure rise curves and matching them against membrane flow capacities. Until then, current H<sub>2</sub> yield estimates may be significantly inflated due to unmodeled feedback inhibition risks during periods of poor headspace ventilation.

### Representative Membrane Materials and Flux Parameters for Hydrogen Separation

This table presents example membrane types, flux characteristics, and performance constraints under vacuum-assisted operation. Values are normalized to STP conditions and 1 atm pressure differential. These benchmarks inform the Membrane Flux Correction Factor (MFCF) applied to theoretical gas clearance rates.

Membrane Type	Material System	Flux (Nm <sup>3</sup> /m <sup>2</sup> /h/bar)	Selectivity (H <sub>2</sub> /CO <sub>2</sub> )	Notes
<b>MOF-Polymer Composite</b>	ZIF-8 in Pebax matrix	0.25 – 0.50	~20 – 30	High-performance lab-scale membranes; sensitive to fouling
<b>Polyimide</b>	Commercial polymer	0.15 – 0.30	~10 – 15	Widely available, thermally stable, moderate selectivity
<b>Silica-Based</b>	Microporous glass	0.10 – 0.20	~5 – 8	Chemically stable, lower selectivity, brittle
<b>PTFE / ePTFE</b>	Expanded Teflon	0.05 – 0.10	~2 – 5	Durable, biofouling-resistant, low separation capacity

Example values sourced from Zhang et al. (2021), Lee et al. (2020), and Li et al. (2019) on hydrogen-selective membrane development. See supplementary materials for extended membrane comparison.

### 5.4.2. Control Systems and Feedback Architecture

Real-time control of environmental parameters is essential for maintaining the functional stability of the dual-stage microbial hydrogen production system. While earlier sections describe a theoretically ideal bioreactor with constant substrate diffusion, light penetration, and anaerobic integrity, real systems require feedback loops to compensate for internal fluctuations, metabolic drift, and external stressors.

This section outlines a modular control strategy designed to monitor and correct deviations in temperature, pH, light intensity, gas accumulation, and CO<sub>2</sub> sequestration rates. All controls are assumed to operate on low-power microcontroller-based platforms (e.g., Arduino, Raspberry Pi) using standard biosensor interfaces.

### 5.4.3. Quantified Hydrogen Accumulation and Inhibition Thresholds:

The inhibitory effects of hydrogen accumulation on enzymatic activity are well-documented in microbial hydrogen systems. Hydrogenase in *Clostridium butyricum* and nitrogenase in *Rhodobacter sphaeroides* exhibit feedback suppression at elevated hydrogen partial pressures, typically around 0.6–0.8 atm. Under the current reactor model, which assumes approximately 12 mol of hydrogen produced over a 72-hour cycle (~0.167 mol/hr), this threshold is reached rapidly if no gas removal occurs.

For a 2-litre reactor with a 0.5-litre gas headspace—a standard design assumption—hydrogen accumulation reaches 0.6 atm partial pressure in less than 5 minutes of continuous production. This corresponds to the accumulation of just ~13.4 mmol of H<sub>2</sub>, based on ideal gas calculations at STP (22.4 L/mol). Without active gas extraction or continuous vacuum cycling, the system would quickly enter a regime of enzymatic inhibition, reducing hydrogen yield and potentially inducing redox or energy stress in the microbial population.

This analysis highlights the critical importance of real-time gas removal or pressure-controlled headspace venting in batch and continuous systems. Future iterations of this model should incorporate hydrogen accumulation kinetics and headspace pressure dynamics to simulate enzyme behaviour more accurately under varying operational conditions.

#### Supporting Calculation: Time to Reach Inhibitory H<sub>2</sub> Pressure

Given:

- Hydrogen production rate: 12 mol / 72 hr = 0.167 mol/hr
- Reactor headspace volume: 0.5 L
- Inhibitory partial pressure threshold: 0.6 atm
- Molar volume at STP: 22.4 L/mol

Required moles of H<sub>2</sub> to reach 0.6 atm in 0.5 L headspace:

$$n = \frac{P \times V}{RT} \approx \frac{0.6 \times 0.5}{22.4} \approx 0.0134 \text{ mol}$$

Time to reach 0.6 atm at constant production:

$$t = \frac{0.0134}{0.167} \approx 0.08 \text{ hour} = 4.8 \text{ minutes}$$

Thus, if hydrogen is not extracted or diffused out of the headspace, the system will exceed the inhibitory threshold in under 5 minutes of operation.

*Side Note:* This model assumes headspace management sufficient to prevent hydrogen accumulation above inhibitory thresholds. Future work will address dynamic gas control strategies to maintain enzymatic activity over extended operation.

#### 5.4.3.1. Core Monitoring Parameters

The following table summarizes the critical control parameters, their sensor types, operating ranges, and programmed responses:

Parameter	Sensor Type	Target Range	Trigger Action
pH (both chambers)	pH probe (glass electrode)	6.2–7.4	<6.0 → alkaline buffer injection; >7.8 → mild acid pulse
Temperature	Thermistor array / RTD	28–32°C	>33°C → Peltier cooling plate or fan activation
Light Intensity (photo chamber)	Photodiode array	25–40 $\mu\text{mol}/\text{m}^2/\text{s}$	<20 → LED boost; >50 → dimming circuit
H <sub>2</sub> Pressure (headspace)	MEMS pressure sensor	<1.1 atm	>1.2 atm → vacuum pump activation
CO <sub>2</sub> Accumulation (in pod)	NDIR gas sensor	<900 ppm	>1000 ppm → alert or temporary gas flow halt
Biofilm Thickness (optional)	Capacitive displacement probe	<1mm	>1.2 mm → alert for manual panel rotation

These sensors ensure system stability without requiring full laboratory automation. All thresholds are programmable and can be adapted per strain tolerance or reactor scale.

#### 5.4.3.2. Control Logic Flow and Safety Behaviour

Each parameter operates within a **hierarchical control loop**, where low-severity deviations trigger passive adjustments (e.g., LED dimming), while high-severity deviations initiate active fail-safes (e.g., CO<sub>2</sub> rerouting or system shutdown).

##### Example Control Chain:

1. **Normal:** Temp = 30°C → stable
2. **Warning:** Temp = 33°C → Fan or TEC turns on
3. **Critical:** Temp = 36°C → LED cutoff + halt fermentation → log error

Fail-safe behaviour includes:

- Auto-throttling of gas flow if CO<sub>2</sub> sensors detect oversaturation in the sequestration pod.
- Redundant pH control with dual dosing pumps to prevent sensor drift-induced pH crash.
- Real-time log file generation for offline diagnostics

Optional software modules can include:

- PID (proportional–integral–derivative) control for smooth system corrections
- Simple logic-based control (if/then) for robustness in off-grid deployments
- GSM or Wi-Fi module for remote alerting and telemetry (for field setups)

#### 5.4.3.3. Suggested Control System Schematic (Textual)

Here is a **verbal schematic** you can translate into a diagram later:

[Biofilm Reactor]



[Sensor Hub]



[Microcontroller Unit]



[Actuator Array]



[Threshold Logic + Timer]



[Data Log]



Feedback Loop

#### Component Descriptions

- **Sensor Hub:** pH, temperature, gas (H<sub>2</sub>/CO<sub>2</sub>), light, biofilm thickness
- **Microcontroller:** Control firmware (e.g., Arduino, Pi)
- **Actuator Array:** Pumps, solenoids, LEDs, cooling fans, TEGs
- **Threshold Logic + Timer:** Evaluates state changes; executes correction routines.
- **Data Log:** Time-stamped CSV or onboard flash storage



#### 5.4.3.4. Deployment Note

While these control systems are low-cost and modular at bench scale, scaling up would require industrial-grade PLCs (programmable logic controllers), multi-channel sensor arrays, and real-time process monitoring dashboards. For field or developing-world setups, simplicity and resilience are prioritized over digital optimization.

#### 5.5. Assumptions and Limitations

- **Uniform substrate diffusion and metabolic activity** are assumed across both biofilms. Nutrient gradients, quorum dynamics, and spatial heterogeneity are excluded from this model.
- **No cross-contamination** or metabolic inhibition is assumed between microbial zones.
- **Light distribution** in the photofermentation chamber is considered sufficient and non-limiting.
- **Vacuum extraction system** is modelled as non-intrusive and energetically lossless, though this remains a significant engineering challenge.

---

#### Author's Note:

A theoretical system cannot be called "complete" if it assumes perfect environmental stability and ignores control infrastructure. These feedback systems not only maintain biological integrity but also function as **ethical enforcers** for the CO<sub>2</sub> redirection requirement, ensuring that industrial misuse cannot bypass sustainability protocols without triggering visible alarms or system throttling.

---

## 6. Biofilm Reactor Architecture and Biomass Scaling

While the primary system modelling in this paper is based on volumetric assumptions (g/L), a growing body of literature supports the use of **biofilm-based reactors** as a superior platform for microbial hydrogen production—particularly under continuous or semi-continuous operation. This section introduces a dedicated biofilm reactor model optimized for *Clostridium butyricum* in the dark fermentation stage, replacing traditional suspension assumptions with surface-area-based biomass density and biofilm-specific engineering parameters.

### 6.1 Rationale for Biofilm Implementation

Biofilm reactors offer several operational and kinetic advantages over suspended systems:

- **Higher effective biomass density** without risk of washout
- **Improved retention time** and microbial longevity
- **Reduced diffusion distance** for substrates and products
- **Lower shear stress** and energy input compared to stirred tanks

These benefits are especially relevant in hydrogen-producing anaerobes like *C. butyricum*, where metabolic performance is sensitive to environmental stability.

### 6.2 Biofilm Biomass Density (g/m<sup>2</sup>)

In contrast to the suspended biomass density of **15 g/L**, biofilm systems are quantified by **dry biomass per unit surface area**. Literature sources report:

- Typical range: **15–25 g/m<sup>2</sup>** [Morimoto et al., 2004]
- Optimized systems: **30–40 g/m<sup>2</sup>**

For equivalent hydrogen output to a 15 g/L suspension system (per litre), a biofilm reactor would require:

That is, **0.5 m<sup>2</sup> of biofilm surface area per litre** of equivalent reactor volume at 30 g/m<sup>2</sup> loading.

### 6.3 Carrier Scaffold Materials and Surface Design

Effective biofilm formation requires scaffold materials that promote microbial adhesion and biofilm stability. Common supports include:

- **Polyurethane foam**: High porosity, low cost
- **Carbon felt**: Chemically stable, high surface roughness
- **Glass beads or mesh**: Inert, reusable
- **Stainless steel mesh**: Rigid and durable, allows heating or conductivity integration

Scaffold geometry (spiral coils, vertical panels, fixed-bed columns) is a critical design parameter, and influences flow distribution and surface accessibility.

## 6.4 Biofilm Limitations and Turnover

Biofilms are not immortal. Long-term operation may encounter:

- **Biofilm degradation** and cell detachment
- **Clogging or uneven flow patterns**
- **Substrate channelling and dead zones**

Productivity usually follows a bell-shaped curve with a lifespan of **2–4 batch cycles (6–10 days)** before requiring panel replacement or regeneration.

## 6.5 Integration with Current Reactor Model

This biofilm adaptation retains the dual-stage design but modifies the dark fermentation chamber to:

- Replace g/L metrics with g/m<sup>2</sup> targets
- Design chamber internals for **≥0.5 m<sup>2</sup>/L** surface exposure
- Use **low-shear recirculation** instead of stirring

Future iterations of this model may fully transition all biomass metrics to surface-area units. For now, this section offers a standalone comparison and integration guideline.

## 6.6 Estimated Biofilm-Based Production Rates for *Clostridium butyricum*

Assuming an optimized biofilm with a **dry biomass density of 40 g/m<sup>2</sup>**, the following process rates are calculated using standard specific activity values for *C. butyricum*:

- **Specific glucose uptake rate (q<sub>s</sub>):** 10 mmol/g/hr
- **Hydrogen yield:** 2 mol H<sub>2</sub>/mol glucose
- **VFA yield:** ~1 mol VFA/mol glucose (primarily butyrate and acetate)

**Per m<sup>2</sup> of biofilm surface:**

- **Glucose consumption:** 10 mmol/g/hr × 40 g = 400 mmol/hr = **72.06 g/hr**
- **Hydrogen production:** 0.4 mol glucose/hr × 2 mol H<sub>2</sub>/mol = **0.8 mol H<sub>2</sub>/hr ≈ 17.93 L H<sub>2</sub>/hr**
- **VFA production:** ~0.4 mol/hr (approx. 0.28 mol butyrate, 0.12 mol acetate)

**Per m<sup>2</sup> per day:**

- **Glucose consumption:** ≈ **1.73 kg/day**
- **Hydrogen production:** ≈ **19.2 mol/day ≈ 430 L H<sub>2</sub>/m<sup>2</sup>/day**
- **Total VFA output:** ≈ **9.6 mol/day**

These rates represent optimized, literature-supported output values under anaerobic, 37°C, pH-stabilized conditions, with sufficient glucose availability and no hydrogen inhibition.

## 6.7 Photofermentative Biofilm Analysis and Butyrate Flux Matching

To fully utilize the butyrate produced by *Clostridium butyricum*, the downstream photofermentative stage must be scaled appropriately to match its VFA output. Based on optimized conditions:

- *Rhodobacter sphaeroides* demonstrates butyrate uptake of ~6 mmol/g/hr under continuous illumination ( $\geq 30 \mu\text{mol}/\text{m}^2/\text{s}$ )
- At a biomass density of **18 g/m<sup>2</sup>**, this corresponds to:

$$6 \text{ mmol}/\text{g}/\text{hr} \times 18 \text{ g} = 108 \text{ mmol}/\text{hr} = 0.108 \text{ mol}/\text{hr}/\text{m}^2$$

- Hydrogen yield from butyrate: **10 mol H<sub>2</sub>/mol butyrate**, yielding:

$$0.108 \text{ mol butyrate}/\text{hr} \times 10 = 1.08 \text{ mol H}_2/\text{hr} = 24.2 \text{ L H}_2/\text{hr}/\text{m}^2$$

### Comparative Butyrate Balance (1 m<sup>2</sup> basis):

- *Clostridium* produces ~0.4 mol/hr of butyrate
- *Rhodobacter* consumes ~0.108 mol/hr of butyrate

To match these rates, the surface area of *Rhodobacter* must be scaled accordingly:

$$\frac{0.4}{0.108} \approx 3.7 \text{ m}^2 \text{ Rhodobacter per m}^2 \text{ Clostridium}$$

This establishes a recommended biofilm surface ratio of:

### 1 : 3.7 (Clostridium : Rhodobacter)

Implementing this ratio prevents VFA accumulation, maintains substrate balance, and ensures uninterrupted hydrogen production across both stages.

## 6.8 CO<sub>2</sub> Output and Biological Fixation Using Sugarcane

To maintain a closed-loop carbon cycle, the CO<sub>2</sub> generated by microbial hydrogen production must be recycled via biological sinks. Both stages—dark fermentation and photofermentation—release CO<sub>2</sub>:

- *Clostridium butyricum* (dark fermentation):  $\text{C}_6\text{H}_{12}\text{O}_6 \rightarrow \text{C}_4\text{H}_8\text{O}_2 + 2\text{CO}_2 + 2\text{H}_2$   
Producing **2 mol CO<sub>2</sub>/mol glucose**  $\rightarrow 0.4 \text{ mol glucose}/\text{hr} \times 2 = \textbf{0.8 mol CO}_2/\text{hr} = \textbf{19.2 mol CO}_2/\text{day}$
- *Rhodobacter sphaeroides* (photofermentation):  $\text{C}_4\text{H}_8\text{O}_2 + 6\text{H}_2\text{O} \rightarrow 10\text{H}_2 + 4\text{CO}_2$   
Consuming 0.4 mol butyrate/day  $\rightarrow \textbf{1.6 mol CO}_2/\text{hr} = \textbf{38.4 mol CO}_2/\text{day}$

**Total CO<sub>2</sub> Output:**  $19.2 + 38.4 = 57.6 \text{ mol CO}_2/\text{day}$

Using controlled greenhouse sugarcane with a **Leaf Area Index (LAI) of 25**, CO<sub>2</sub> fixation is:

$$32.5 \mu\text{mol}/\text{m}^2/\text{s} \times 36,000 \text{ s}/\text{day} = 1.17 \text{ mol CO}_2/\text{m}^2/\text{day}$$

$$1.17 \text{ mol} \times 25 = 29.25 \text{ mol CO}_2 \text{ fixed}/\text{m}^2/\text{day}$$

To fully capture 57.6 mol CO<sub>2</sub>/day, the required sugarcane ground area is:

$$\frac{57.6}{29.25} \approx 1.97 \text{ m}^2$$

Thus, **1.97 m<sup>2</sup> of sugarcane**, under optimal photosynthetic conditions, is sufficient to offset the CO<sub>2</sub> emissions of the entire system, achieving **net-zero or negative-carbon operation**.

### 6.9 Comparative Yield Assessment: Suspension vs. Biofilm Reactor

To quantify the improvement introduced by transitioning from a suspension-based design to a biofilm system, the following comparative assessment is made:

#### Suspension Reactor (5.5 L total volume):

- *Clostridium* chamber: 1 L @ 15 g/L
- *Rhodobacter* chamber: 3.125 L @ 6 g/L (scaled to match VFA flux)
- Total H<sub>2</sub> output:
  - *Clostridium*: 0.3 mol/hr × 24 = **7.2 mol/day**
  - *Rhodobacter*: 1.125 mol/hr × 24 = **27 mol/day**
  - **Total: 34.2 mol H<sub>2</sub>/day ≈ 766 L/day**

#### Biofilm Reactor (1 m<sup>2</sup> *Clostridium* + 3.7 m<sup>2</sup> *Rhodobacter*):

- *Clostridium* biofilm: 40 g/m<sup>2</sup>
- *Rhodobacter* biofilm: 18 g/m<sup>2</sup>
- Total H<sub>2</sub> output:
  - *Clostridium*: 0.8 mol/hr × 24 = **19.2 mol/day**
  - *Rhodobacter*: 4 mol/hr × 24 = **96 mol/day**
  - **Total: 115.2 mol H<sub>2</sub>/day ≈ 2581 L/day**

**Improvement Factor:**  $\frac{115.2}{34.2} \approx 3.37 \times \text{increase in } H_2 \text{ yield}$

This comparison demonstrates that, at equivalent metabolic configurations and substrate supply, the biofilm system achieves over **3× higher hydrogen yield** with superior stability, scalability, and integration potential.

## 7. Gas Separation and Post Processing

The dual-stage microbial hydrogen production process yields a gaseous mixture composed primarily of hydrogen (H<sub>2</sub>) and carbon dioxide (CO<sub>2</sub>), which must be separated efficiently to preserve product purity and enable sustainable downstream processing. This section outlines the theoretical gas separation mechanism employed in the model and its associated assumptions.

### 7.1. Membrane Separation

The system uses a vacuum-assisted membrane separation module designed to selectively extract hydrogen from the fermentation headspace. Hydrogen is extracted first due to its high diffusivity and favourable permeation properties in most polymer membranes. While molecular size plays a role, effective separation depends on the selectivity of the membrane material and the partial pressure differential across it. For this model, two classes of membranes are considered:

- **Polyimide-based membranes:** Common in gas separation, offering moderate H<sub>2</sub>/CO<sub>2</sub> selectivity and high mechanical stability.
- **Metal-Organic Frameworks (MOFs):** Emerging materials with tuneable pore sizes and potentially higher selectivity, modelled here as a theoretical performance benchmark [5].

Vacuum pressure is applied across the membrane surface to enhance gas flux. The system is assumed to operate under thermally stable, anaerobic conditions to prevent oxidation and enzymatic inhibition. While modelled here as perfectly staged and non-overlapping, each membrane step in real systems results in partial gas mixing. Recirculation loops, pressure swing adsorption, or cryogenic polishing may be required to achieve the purity assumed in the current idealized model.

#### 7.1.1. Membrane Lifespan, Degradation, and Fouling Considerations

The gas separation system in this model utilizes semi-permeable vacuum-assisted membranes for hydrogen and CO<sub>2</sub> extraction. While theoretical performance assumes >95% separation efficiency, practical implementations face performance drift due to material degradation, physical stress, and fouling from microbial byproducts.

Key degradation and fouling risks include:

- **Protein Mist Fouling:** Fine droplets from active fermentation can condense on membranes, blocking pores and reducing flow rate.
- **Salt Crystallization:** Trace ionic species in the broth may vaporize and deposit on membranes, especially in long-cycle or high-CO<sub>2</sub> environments.
- **Vacuum Fatigue:** Repeated vacuum cycling induces microfractures and pore deformation, particularly in polymer-based membranes.
- **Acidic Gas Corrosion:** CO<sub>2</sub>-rich gas streams can lower pH and erode polymeric layers over multiple cycles if not buffered.

Stressor	Primary Effect	Degradation Onset (Est.)	Mitigation
Biofilm mist / protein fog	Pore clogging	24–48 h	Pre-filtration mesh, vertical flow path
CO <sub>2</sub> acidification	Polymer erosion	5+ cycles	Use of fluoropolymer or ceramic layers
Vacuum cycling	Micro-fracturing	~30–50 cycles	Lower vacuum pulsing frequency
Salts / metabolites	Crystallization/fouling	48–72 h	Gas polishing (desiccant + filter)

To simplify modelling, this system assumes no membrane replacement within a 72-hour cycle, with a conservative performance loss margin of **≤5%** factored into gas recovery estimates. For continuous or extended-cycle setups, performance decay should be modelled dynamically, and **membrane health sensors or differential flow detection** can be integrated for predictive maintenance.

Future iterations may benefit from pre-filtration chambers, dedicated gas polishing columns, and switchable membrane banks for redundancy.

### 7.1.2. Membrane Throughput Constraints and Gas Flux Limitations

While membrane-based gas separation systems offer scalable selectivity and moderate energy requirements, real-world performance is ultimately constrained by membrane area, gas flux rate, and partial pressure differentials. In the current model, gas extraction is treated as continuous and instantaneous, with all hydrogen produced (12 mol per cycle) assumed to be removed in real time. However, without quantifying membrane throughput (typically expressed in Nm<sup>3</sup>/m<sup>2</sup>/h/bar), the system risks hydrogen accumulation in the headspace—potentially surpassing the inhibitory threshold for hydrogenase and nitrogenase activity (~0.6 atm).

To prevent enzymatic suppression, future designs must benchmark membrane surface area, permeability coefficients, and operational pressure differentials to ensure adequate volumetric flow rates. If extraction lags gas production, internal feedback inhibition may compromise yield regardless of stoichiometric potential.

### 7.1.3. Gas Purity and Post-Separation Polishing

Although the current model assumes hydrogen purity suitable for energy applications, typical membrane separations alone do not meet the ≥99.97% purity threshold required for polymer electrolyte membrane fuel cells (PEMFCs). Even with a 92% selectivity rate, trace CO<sub>2</sub>, water vapor, and residual metabolites may remain in the product stream. Realistic systems may therefore require secondary polishing units—such as pressure swing adsorption (PSA), catalytic oxidation beds, or activated carbon filters—to achieve fuel-grade standards. These components are omitted from this model but should be considered in lifecycle design for application-specific deployment.



#### 7.1.4. Backpressure and Vacuum-Induced Stress Considerations

Vacuum-assisted separation introduces negative pressure differentials across the membrane and reactor headspace. While the model assumes this extraction occurs without disrupting internal microbial dynamics, real-world systems may experience shear stress on biofilm surfaces, altered gas solubility, or microbially relevant pressure fluctuations. These shifts could destabilize biofilm attachment or impair metabolic output. Future iterations should consider pressure dampeners, buffer chambers, or variable-flow regulators to mitigate these risks and preserve system integrity during extended operation.

### 7.2. CO<sub>2</sub> Routing and Sink Options

For theoretical yield benchmarking, this model assumes best-case performance for membrane gas separation. However, to contextualize feasibility, a realistic performance corridor is also described below.

- **Hydrogen/CO<sub>2</sub> separation efficiency:**  
Modelled at **100%** for theoretical ceiling, but real-world membrane recovery rates range from **85–95%** depending on material, pore stability, and backpressure control [Bernardo et al., 2009].
- **Membrane lifespan:**  
Idealized as indefinite, but real systems experience **biofouling, pore compaction, and selectivity loss** over time. Cleaning cycles or replacements every **300–500 hours** are common.
- **Vacuum extraction loss:**  
Assumed lossless, but actual systems incur **5–15% efficiency penalties** due to pump inefficiency, heat loss, or pulsed extraction behaviour.
- **Product purity:**  
Fuel-grade H<sub>2</sub> is assumed, but in practice **polishing steps** like pressure swing adsorption (PSA), activated carbon filters, or moisture traps may be required.

These constraints are not simulated in this model but must be considered for realistic deployment. Future extensions may incorporate fouling coefficients, separation efficiency decay curves, and energy cost scaling with purity thresholds.

#### 7.2.1. Yield Impact from Separation Losses

To quantify the effect of real-world membrane inefficiencies on hydrogen recovery, a comparative energy yield analysis was conducted.

Assumptions:

- Theoretical H<sub>2</sub> production per cycle = **12 mol**
- Combustion energy per mol H<sub>2</sub> = **286 kJ/mol**
- Ideal separation efficiency = **100%**
- Realistic separation efficiency = **92%** (typical for polymer/MOF hybrid membranes)

### Energy loss from H<sub>2</sub> capture inefficiency:

$$\text{Captured } H_2 = 12 \text{ mol} \times 0.92 = 11.04 \text{ mol}$$

$$\text{Recovered Energy} = 11.04 \text{ mol} \times 286 \text{ kJ/mol} \approx 3157.4 \text{ kJ}$$

Compared to the ideal yield of **3432 kJ**, this is a **loss of 274.6 kJ**, or **~8% energy penalty** purely from imperfect gas separation.

**Impact on Net Energy Gain:** Original net gain = 3432 – 960 = **2472 kJ**

Adjusted net gain = 3157.4 – 960 = **2197.4 kJ**

→ **Net energy drop: ~11.1%**

This demonstrates that even modest membrane inefficiencies can meaningfully reduce system energy balance. For scaled systems, such losses may justify staged membrane banks or polishing units to preserve fuel-grade output.

### 7.2.2. CO<sub>2</sub> Recycling Efficiency via Sugarcane Integration

To offset carbon emissions from the dual-stage microbial hydrogen reactor, a photosynthetic carbon fixation module is proposed using **high-efficiency C<sub>4</sub> sugarcane** as a biological sink. This section quantifies the amount of CO<sub>2</sub> released by the system and calculates the spatial requirements of sugarcane necessary to fully recycle it.

#### CO<sub>2</sub> Emissions from 5.5 L Reactor

The 5.5 L hydrogen production system comprises:

- **1.0 L Clostridium butyricum** chamber
- **3.125 L Rhodobacter sphaeroides** chamber
- **~0.375 L for buffering, flow, and headspace**

Based on known glucose-to-hydrogen fermentation stoichiometry:

- Each mole of glucose yields 2 mol CO<sub>2</sub> during dark fermentation
- The Clostridium stage consumes ~9 mol glucose/day to generate 18 mol H<sub>2</sub>

Thus, daily CO<sub>2</sub> output:

$$9 \text{ mol glucose/day} \times 2 = 18 \text{ mol CO}_2/\text{day}$$

$$18 \text{ mol} \times 22.4 \text{ L/mol} = 403.2 \text{ CO}_2/\text{day}$$

The Rhodobacter stage contributes negligible CO<sub>2</sub> under ideal photofermentation conditions, as VFAs are converted to hydrogen and acetate without significant carbon loss.

## Sugarcane CO<sub>2</sub> Fixation Capacity

Sugarcane is a high-efficiency C<sub>4</sub> crop with exceptional photosynthetic throughput. In this model, the sugarcane is cultivated in a **controlled greenhouse environment**, eliminating seasonal variation and ensuring consistent CO<sub>2</sub> uptake. Under adequate artificial or solar-assisted lighting (10 hours/day), sugarcane leaf tissue fixes CO<sub>2</sub> at a rate of ~32.5 μmol/m<sup>2</sup>/s. A 5-meter-tall sugarcane plant exhibits a high **Leaf Area Index (LAI)**, estimated at ~25 due to multiple vertical leaves and overlapping canopies.

Fixation calculation:

$$32.5 \mu\text{mol}/\text{m}^2/\text{s} \times 36,000 \text{ s}/\text{day} = 1.17 \text{ mol CO}_2/\text{m}^2/\text{day}$$

$$1.17 \text{ mol} \times 25 = 29.25 \text{ mol CO}_2 \text{ fixed}/\text{day}/\text{m}^2$$

$$29.25 \text{ mol} \times 22.4 \text{ L}/\text{mol} = 655.2 \text{ L CO}_2/\text{day}/\text{m}^2$$

## Matching Reactor CO<sub>2</sub> Emissions

To neutralize the CO<sub>2</sub> output of the 5.5 L reactor (403.2 L/day):

$$403.2 \div 655.2 = 0.615 \text{ m}^2$$

Thus, less than **0.62 m<sup>2</sup>** of sugarcane cultivation is needed to offset the entire CO<sub>2</sub> output of the prototype system.

## Conclusion

A small panel of sugarcane (~0.62 m<sup>2</sup>) with 5-meter stalks is sufficient to fully recycle CO<sub>2</sub> emissions from the 5.5 L hydrogen reactor, achieving **net-zero or negative-carbon operation**. This integration confirms the feasibility of biologically closed-loop hydrogen production at lab and industrial scales when coupled with high-yield carbon-fixing crops.

### 7.3. System Losses and Gas Fate

This section assumes best-case membrane function for modelling clarity. In real-world systems, gas separation faces multiple engineering constraints including:

- Partial pressure gradients that limit flux across membranes.
- Membrane aging and fouling from bioaerosols or organic residues.
- Backpressure that could affect gas accumulation rates or microbial equilibrium.
- Vacuum system inefficiencies, such as pulsed flow, heat buildup, and non-linear extraction rates.

While these effects are not modelled here, they present clear avenues for future investigation. For instance, hydrogen recovery efficiencies in real systems often fall between 85–95%, and energy requirements for vacuum pumps scale non-linearly with extraction volume and purity targets. Additionally, pressure differential stress across biofilms could lead to microbial adhesion loss or diffusion barriers, requiring pressure dampening designs in future prototypes. These challenges reinforce the need for experimental membrane characterization, CFD simulation of gas flow, and pressure-regulated biofilm integration in scaled systems. Until such data becomes available, the present model defines an upper-bound, zero-loss gas separation baseline.

To further clarify the performance gap between the idealized membrane model and real-world system behaviour, this table summarizes critical membrane and vacuum gas handling parameters, with estimated realistic performance ranges and their impact on system operation.

Parameter	Ideal Model	Realistic Range	Impact
H <sub>2</sub> Separation Efficiency	100%	85-95%	Lowers product yield, energy recovery
Vacuum Pump Efficiency	100%	85-90%	Increases power draw
Membrane Lifetime	Infinite	300-500 Cycles	Affects maintenance and cost
Biofouling	None	Mild-Moderate	Requires cleaning cycles
Purity (H <sub>2</sub> %)	100%	93-98%	May need PSA or polishing

## 8. CO<sub>2</sub> Fixation and Redirection Strategy

The dual-stage microbial system yields significant volumes of carbon dioxide as a metabolic byproduct—estimated at **6 mol CO<sub>2</sub> per mole of glucose**, or approximately **264 g CO<sub>2</sub> per 180.16 g glucose**, resulting in a CO<sub>2</sub>-to-glucose mass ratio of **146.56%**. This value exceeds the substrate mass due to oxygen atoms derived from water during photofermentation reactions. To maintain environmental sustainability, the model emphasizes redirecting this CO<sub>2</sub> to biological carbon sinks.

### 8.1. Candidate Biological Sinks

Three primary biological systems are proposed for CO<sub>2</sub> assimilation:

#### 8.1.1. Sugarcane Plantations (C<sub>4</sub> Crops)

- High CO<sub>2</sub> fixation rates
- Dual purpose: sequestration + potential glucose recovery
- Proven viability in tropical and subtropical zones

#### 8.1.2. Bamboo Forests

- Among the fastest-growing terrestrial plants
- High year-round carbon uptake per hectare
- Suitable for industrial land reclamation or buffer zones

#### 8.1.3. Algae Bioreactors [8]

- High surface area to volume ratio for CO<sub>2</sub> uptake
- Suitable for urban, modular, or space-limited deployment
- Biomass can be harvested for nutrient recovery or biofertilizer.

Other systems like aquatic plant ponds (e.g., duckweed) were explored but deprioritized due to acidification risks and high maintenance needs for pH stabilization.

### 8.2. Storage and Transport Assumptions

Separated CO<sub>2</sub> is assumed to be stored at ambient pressure in intermediate buffer tanks before redirection. No liquefaction or compression is modelled. Transport to biological sinks is assumed to occur via insulated pipelines or short-range pressure vessels depending on site layout and distance. These assumptions are idealized and exclude energy or infrastructure costs.

### 8.3. Scientific Frustrations and Realism Acknowledgement

While the paper outlines multiple CO<sub>2</sub> fixation strategies, achieving a truly closed-loop carbon system is far from straightforward. Each sink presents trade-offs:

- **Land-based sinks** (sugarcane, bamboo) demand significant space, irrigation, and land-use planning.
- **Algal systems** require strict environmental control (light, nutrients, mixing) and capital investment.
- **Aquatic sinks**, though attractive, suffer from ecosystem acidification without alkaline buffering.

Moreover, the actual CO<sub>2</sub> uptake efficiency of each system is highly variable and context dependent. Climate, crop health, microbial symbiosis, and system maintenance all contribute to sequestration inconsistency.

This section represents a combination of plausible strategies and educated speculation. While redirecting CO<sub>2</sub> biologically is possible, it is also clear that implementation would require site-specific optimization, lifecycle cost analysis, and multi-disciplinary collaboration. The paper emphasizes this limitation as one of the most significant engineering and ecological challenges in making microbial hydrogen production truly carbon neutral.

#### 8.3.1. Temporal and Lifecycle Constraints in CO<sub>2</sub> Fixation

While this model proposes redirecting CO<sub>2</sub> emissions into high-efficiency biological sinks such as sugarcane plantations, algae bioreactors, and bamboo forests, it currently treats these systems as **instantaneous and lossless carbon absorbers**. In practice, **CO<sub>2</sub> fixation is delayed, variable, and biologically constrained** by multiple factors:

Factor	Effect on CO <sub>2</sub> Fixation
<b>Growth Phase</b>	Young or senescent plants fix less CO <sub>2</sub> than those in peak growth
<b>Climate &amp; Light</b>	Reduced fixation under low light, drought, or temperature extremes
<b>Nighttime Respiration</b>	Plants respire CO <sub>2</sub> during darkness, offsetting net capture
<b>Soil and Root Limitations</b>	Poor soil health or root stress can limit nutrient uptake, slowing CO <sub>2</sub> assimilation
<b>Algal Turnover</b>	Bioreactor systems require regular harvesting or risk CO <sub>2</sub> saturation and stalling

*Implication:* Even with optimal gas routing, **real-time CO<sub>2</sub> absorption may lag emission**, resulting in **temporary atmospheric accumulation** unless properly buffered.

To address this, future models should include:

- **Lag curves** to model sequestration delay vs. emission rate.
- **CO<sub>2</sub> buffer tanks** or regulated injection pacing
- Lifecycle-based tracking of **plant biomass carbon retention** vs. turnover or decay

**Net-zero status** should be assessed over longer periods (e.g., weekly/monthly) rather than per-cycle, acknowledging that biological sinks accumulate CO<sub>2</sub> gradually, not on demand.

### 8.3.2. Lifecycle Carbon Accounting and Sink Saturation Limitations

While this model treats CO<sub>2</sub> redirection as an environmentally positive strategy, a complete life-cycle carbon budget remains outside the current scope. Key variables such as plant respiration, post-harvest biomass decay, transport emissions, and land-use change are not modelled. As such, carbon neutrality is evaluated at the point of CO<sub>2</sub> injection into the biological sink, not the full assimilation and retention pathway. This creates a temporal and spatial mismatch between emission and sequestration, which may be acceptable in short-cycle systems but problematic at industrial scale.

Moreover, all candidate sinks—sugarcane, bamboo, and algae—have upper limits on their CO<sub>2</sub> fixation capacity. Algae bioreactors, for instance, can become saturated within 24–48 hours if biomass is not harvested regularly, while sugarcane plantations exhibit declining CO<sub>2</sub> uptake as atmospheric concentrations plateau near the plant's physiological maximum (~500 ppm in localized zones). None of these dynamic limitations are currently simulated in this version of the model.

Future implementations should include saturation response curves, storage buffer capacities, and CO<sub>2</sub> pacing algorithms to prevent over-saturation, backflow, or temporal CO<sub>2</sub> buildup. This is particularly important in closed loop or semi-autonomous installations where manual oversight is limited. Additionally, routing infrastructure—assumed here to be lossless and energetically neutral—should be evaluated for compression costs, leak risk, and maintenance overhead in long-distance or industrial deployments.

#### Clarification on Temporal Lag in CO<sub>2</sub> Sequestration:

While this model assumes that carbon dioxide emissions from microbial metabolism are routed to external biological sinks such as sugarcane plantations or algae bioreactors, it currently treats sequestration as temporally immediate and lossless. In real ecosystems, CO<sub>2</sub> uptake is delayed by biological growth cycles, seasonal variation, and environmental stressors. For example, sugarcane exhibits peak fixation rates only during active vegetative growth, with significantly reduced carbon assimilation during early growth or senescence phases. Likewise, algae systems may saturate with CO<sub>2</sub> under suboptimal light or nutrient depletion, introducing lag between gas delivery and biomass conversion.

Therefore, while the model achieves theoretical carbon neutrality on a per-cycle basis, actual atmospheric offsetting will occur over extended timescales—days to weeks for algae systems, and weeks to months for land-based crops. This temporal mismatch may result in transient CO<sub>2</sub> accumulation unless buffered via intermediate gas storage or throttled injection rates. Future models should integrate sequestration lag curves and dynamic sink response profiles to represent net-zero trajectories more accurately over realistic operational timelines.



---

### Terminology Note: Distinction Between Biomass Types

In this paper, the term **biomass** is used in two distinct biological contexts. To avoid confusion, the following terminology is applied throughout:

- **Microbial Biomass** (also referred to as *cellular biomass*): Refers to the accumulation of bacterial or phototrophic cell mass during fermentation. This includes protein, lipids, DNA/RNA, and structural polysaccharides formed from substrate carbon.
- **Plant Biomass** (also referred to as *sugarcane biomass* or *CO<sub>2</sub> sink biomass*): Refers to vegetative tissue formed by C<sub>4</sub> plants like sugarcane as part of the system's carbon fixation loop.

When yield metrics refer to "**biomass diversion**" or "**Biomass Diversion Factor (BDF)**", they pertain to **microbial biomass only**—not plant tissue.

This distinction ensures clarity in carbon accounting, resource budgeting, and life-cycle assessments across both fermentation and sequestration components.

---

## 9. Theoretical Results and Yield Modelling

This section consolidates the theoretical stoichiometric outcomes of the dual-stage microbial hydrogen production system. Calculations are based on idealized assumptions of complete substrate conversion, lossless gas extraction, and unrestricted enzyme performance.

### 9.0.1. Unit Legend

To ensure consistency across all energy, yield, and cost metrics presented in this paper, the following unit conventions are applied:

- **Energy** values are expressed in **kilojoules (kJ)**. For readability, values exceeding 1000 kJ are also reported in **megajoules (MJ)**, where:

$$1 \text{ MJ} = 1000 \text{ kJ}$$

- **Hydrogen** quantities are provided in both **moles (mol)** and **grams (g)**. The molar mass of hydrogen is taken as **2.02 g/mol**.
- **Carbon dioxide (CO<sub>2</sub>)** outputs are reported in **grams (g)**, based on a molar mass of **44.01 g/mol**.
- **Gas volumes** are calculated at **Standard Temperature and Pressure (STP)**, defined in this model as **0°C and 1 atm**, with a molar volume of **22.4 L/mol**. Deviations due to temperature and pressure are not modelled in this version.
- **Cost values** are reported in **U.S. dollars (USD)** and are based on industrial utility rates and bulk glucose pricing within the United States.

All tables and quantitative outputs from **Section 8 onward** adopt these units unless otherwise specified. This standardization supports comparative interpretation, external benchmarking, and ease of conversion across related studies.

### 9.0.2. Yield Metrics Terminology

Metric	Definition	Example
<b>Mass Yield (%)</b>	Percentage of hydrogen mass relative to input substrate mass.	24.24 g H <sub>2</sub> from 180.16 g glucose = <b>13.45%</b>
<b>Energy Yield (kJ / MJ)</b>	Total energy content of hydrogen produced based on 286 kJ/mol H <sub>2</sub> .	12 mol H <sub>2</sub> = <b>3432 kJ = 3.43 MJ</b>
<b>Energy Efficiency (%)</b>	Ratio of energy output to total system input. Two forms are used: NEF and EROIE.	NEF = <b>78.1%</b> ; EROIE = <b>3.58</b>
<b>Yield by Input Basis</b>	Reference used for input mass: glucose-only, glucose + water, or butyrate + water.	Mass yield = 13.45% (glucose), 8.41% (glucose + water)
<b>Volumetric Productivity</b>	Hydrogen volume produced per litre of reactor volume per day (L/L/day).	<b>44.85 L/L/day</b>
<b>Areal Productivity</b>	Hydrogen volume produced per square meter of light-exposed surface area per day (L/m <sup>2</sup> /day).	<b>~1120 L/m<sup>2</sup>/day</b>
<b>Carbon-to-CO<sub>2</sub> Ratio</b>	Total CO <sub>2</sub> output mass relative to input glucose mass, reflecting oxidation extent.	264.06 g CO <sub>2</sub> from 180.16 g glucose = <b>146.56%</b>
<b>Net Energy Gain (kJ)</b>	Energy output minus system input, accounting for ideal or real-world losses.	<b>2472 kJ</b> net gain at theoretical max

These standardized definitions are referenced across stoichiometric, energetic, and kinetic sections to ensure consistency and clarity.

#### Clarification on Energy Efficiency Metrics:

Two forms of energy efficiency are used throughout this paper:

- **Net Energy Fraction (NEF)** = Output Energy / (Output + Input)
  - **Energy Return on Input Energy (EROIE)** = Output Energy / Input
- These definitions provide complementary perspectives on system performance, reflecting both absolute and relative energy returns.

### 9.1. Yield Summary

Starting from 1 mol glucose, the system yields 12 mol H<sub>2</sub> (2 from dark fermentation and 10 from photofermentation), with 6 mol water consumed. This equals **13.45% mass yield (glucose only)** or **8.41% (glucose + water)**.

Stage	H <sub>2</sub> Produced	Yield by Mass (Input Basis)
Dark Fermentation	2 mol	2.24% (per mol glucose)
Photofermentation	10 mol	10.29% (per mol butyrate + water)
<b>Total (per cycle)</b>	<b>12 mol</b>	<b>13.45% (glucose only) / 8.41% (glucose + water)</b>

### Substrate Contribution to Energy Yield (Not Mass-Based)

Input Component	Input Mass (g)	Role	Energy Contribution
Glucose	180.16	Primary fermentable substrate; donor of electrons and carbon	~100% of caloric energy input
Water	108.09	Electron donor during photofermentation; contributes hydrogen atoms but no caloric energy	~0% (non-energetic, non-combustible)

#### Clarification on Water's Role:

Water contributes **hydrogen atoms**, not caloric energy. During photofermentation, water serves as an **electron donor** whose hydrogen atoms are split via light-driven nitrogenase activity. However, this process does **not provide chemical energy**—only electrons and protons. Therefore, the system's **entire energy yield originates from glucose oxidation**, even though the total **hydrogen yield** includes atoms from both glucose and water.

*Side Note:* While water provides hydrogen atoms for photofermentation via light-driven nitrogenase activity, it does not contribute any usable energy in the form of enthalpy. The entire system's energy output derives from glucose oxidation alone. Any reference to “yield including water” reflects mass-based input comparisons, not energy sources.

While the total mass input includes both glucose and water, their contributions to energy output are not equivalent. Glucose serves as the primary energy substrate, whereas water functions as a hydrogen donor with negligible caloric value but serving as a critical electron donor in photofermentation. This table clarifies the input components' roles in the system's energy yield.

#### Clarification on Yield Metrics:

While mass yield is a convenient metric for comparing biochemical conversion efficiency, hydrogen is primarily valued as an energy carrier. Therefore, energy-normalized yields (e.g., MJ per mol substrate) provide a more meaningful basis for system benchmarking and economic comparison. Mass-based values are still included to enable direct comparison with microbial and enzymatic yield literature, where this format remains common.

- **Molar mass of H<sub>2</sub>:** 2.02 g/mol
- **Total H<sub>2</sub> mass:** 12 mol × 2.02 g/mol = **24.24 g**
- **Total input mass:** 180.16 g (glucose) + 108.09 g (water) = **288.25 g**

**Yield Basis Clarification:** Hydrogen yield can be expressed using multiple mass-based references, depending on whether input mass includes only the primary substrate or all reactants. This model provides three key perspectives for clarity:

Yield Basis	Input Mass (g)	H <sub>2</sub> Produced (g)	Mass Yield (%)	Notes
Glucose only	180.16	24.24	13.45	Traditional metric in microbial literature
Glucose + Water	180.16 + 108.09 = 288.25	24.24	8.41	Reflects total input mass for full-cycle fermentation
Butyric Acid + Water	88.11 + 108.09 = 196.20	20.20	10.29	Applies to photofermentation stage only

Each format is useful depending on whether the analysis focuses on:

- Substrate-to-product conversion (glucose-only)
- Total resource consumption (glucose + water)
- Stage-specific yield (butyrate + water)

These yield values are based on complete conversion assumptions and are recalculated in adjusted form later using BDF and BRV values in Section 8.3.2.

### 9.1.1. H<sub>2</sub> Yield Sensitivity

To illustrate system variability under suboptimal conditions, this table presents a range of hydrogen yields and their associated energy and efficiency impacts. These values help define a realistic operating envelope for future system iterations.

#### Note on Efficiency Units:

All efficiency values in the following table are calculated based on a **fixed input energy of 960 kJ per cycle**, reflecting the theoretical system energy requirement under ideal conditions. These values represent **apparent system efficiency**, assuming consistent operation time and energy expenditure per batch.

In practical systems, energy input may scale dynamically with process duration, hydrogen yield, or system throttling. For this reason, a separate table modelling **scaled input efficiency** is provided in Section 8.3.2. This distinction ensures clarity between **static efficiency benchmarking** and **adaptive, yield-dependent energy analysis**.

H <sub>2</sub> Yield (mol)	H <sub>2</sub> Energy Output (kJ)	Net Energy Gain (kJ)	Apparent System Efficiency (%)	H <sub>2</sub> Yield by Mass (%)
12	3432 (3.43 MJ)	2472	78.14	13.45
10	2860	1900	74.87	11.21
8	2288	1328	70.44	8.97
6	1716	756	64.13	6.73

## Efficiency Under Scaled Input Conditions (Projected)

This table models dynamic input scaling based on hydrogen output, assuming the system runs for shorter durations or uses less power when yield is reduced. It shows that efficiency does not drop sharply if energy input is adjusted proportionally.

H <sub>2</sub> Yield Sensitivity	H <sub>2</sub> Energy Output	Scaled Input Energy (kJ)	Net Energy Gain (kJ)	Scaled System Efficiency (%)
12	3432	960	2472	78.1
10	2860	800	2060	72.0
8	2288	640	1648	71.8
6	1716	480	1236	71.6

### 9.1.2. CO<sub>2</sub> Output Analysis

- **CO<sub>2</sub> Produced:** 6 mol per mol glucose.
- **Molar mass of CO<sub>2</sub>:** 44.01 g/mol
- **Total CO<sub>2</sub> mass:** 6 × 44.01 = **264.06 g**
- **CO<sub>2</sub>-to-glucose mass ratio:** (264.06 / 180.16) × 100 ≈ **146.56%**

*Side Note:* For earlier discussion of oxygen contribution from water molecules, see Section 3.4.

## 9.2. Modelling Assumptions

- Full conversion of substrate to desired products
- Ideal anaerobic conditions, optimal temperature (37°C), and sufficient light intensity
- No gas loss, contamination, or membrane inefficiency
- Biofilm performance is spatially uniform.

These theoretical outcomes represent upper-bound estimates. Real-world yields may vary due to substrate limitations, microbial kinetics, enzyme inhibition, or incomplete gas capture, all of which are excluded from this model for simplicity and clarity.

## 9.3. Sensitivity Considerations and Yield Variability

While this model reports a theoretical hydrogen yield of 12 mol H<sub>2</sub> per glucose cycle under ideal conditions, real-world systems rarely achieve perfect conversion. Key process variables—including substrate concentration, light intensity, microbial activity, and gas separation efficiency—can introduce significant variability.

For instance, a 20–30% reduction in photofermentation efficiency (e.g., due to suboptimal lighting or VFA buildup) would lower total hydrogen yield to ~9–10 mol H<sub>2</sub> per cycle. Similarly, incomplete CO<sub>2</sub> separation or membrane fouling could reduce effective gas collection rates, impacting the net energy recovery and skewing cost estimates.

In energy terms, a drop from 12 mol H<sub>2</sub> to 9 mol would reduce gross energy output from ~3.43 MJ to ~2.57 MJ—cutting net energy gain by nearly 25%.

These outcomes highlight the importance of system robustness, adaptive control mechanisms, and experimental optimization. While this paper establishes a theoretical upper-bound, future models should incorporate probabilistic ranges, confidence intervals, or empirical yield curves to better represent operational variability.

### 9.3.1. Yield Realism Gradient

To contextualize the theoretical yield of 12 mol H<sub>2</sub> per mole of glucose, a performance gradient is presented below. This stratification illustrates hydrogen yield performance under progressively realistic constraints, ranging from idealized models to conservative real-world outcomes.

Scenario	H <sub>2</sub> Yield (mol)	Description
Theoretical Ceiling	12	Assumes complete glucose and VFA conversion, no biomass generation, no energy loss, and perfect enzyme expression.
Optimized System	10	Partial VFA conversion (~85–90%), minimal diversion into biomass, high metabolic efficiency.
Practical High-End	8	Includes biomass formation (10–15%), moderate kinetic losses, and less efficient light or nutrient use.
Conservative Estimate	6	Reflects experimental averages with significant VFA retention, non-optimized strains, and real-world kinetic bottlenecks.

### 9.3.2. Biomass Corrected Yield Estimates

Scenario	BDF (%)	BRF (%)	Effective H <sub>2</sub> Yield (mol)	Energy Output (kJ)	Efficiency (%)	Yield by mass (%)
Theoretical Max	0	1.00	12	3432	78.14	13.45
Moderate Biomass	10	0.90	10.8	3080	74.2	12.11
Realistic Field	20	0.80	9.6	2746	70.0	10.76
Conservative	30	0.75	9.0	2574	67.3	10.08

These estimates assume proportional diversion of glucose- and VFA-derived carbon into non-gas biomass structures. This includes amino acids, nucleotides, and structural polysaccharides. Although the degree of biomass formation depends on nutrient conditions, reactor cycling, and microbial growth phase, empirical studies support a diversion range of 10–30% in batch systems [3].

*Side Note:* Adjusted hydrogen yields in this table are derived by estimating carbon diversion from glucose into microbial biomass. As biomass retains significant substrate carbon, this diversion directly reduces the number of carbon atoms oxidized to CO<sub>2</sub> during photofermentation. Since hydrogen production in *R. sphaeroides* is stoichiometrically linked to CO<sub>2</sub> evolution, yield losses are approximated proportionally based on carbon retention assumptions. Further refinement using empirical carbon flux analysis is planned in future models.



### 9.3.2.1. Carbon Diversion and Impact on H<sub>2</sub> Yield

In the dual-stage model, hydrogen yield is tightly coupled to the **oxidation of glucose-derived carbon atoms**. Each mole of glucose (C<sub>6</sub>H<sub>12</sub>O<sub>6</sub>) contains six carbon atoms. Under ideal, complete oxidation:

- 2 carbon atoms are released as CO<sub>2</sub> during dark fermentation.
- The remaining 4 carbon atoms are released during photofermentation of butyric acid.

Because photofermentative hydrogen production by *Rhodobacter sphaeroides* is stoichiometrically linked to CO<sub>2</sub> evolution—with an approximate **2:1 molar ratio of H<sub>2</sub> to CO<sub>2</sub>**—any carbon **retained in biomass** instead of being oxidized results in a proportional **loss of H<sub>2</sub> yield**.

#### Hydrogen Yield Equation (BDF-Corrected):

To account for the diversion of substrate carbon into microbial biomass, the following formula calculates the total hydrogen yield per mole of glucose based on the **Biomass Diversion Factor (BDF)**.

Let **x** represent the fraction of carbon atoms from glucose that are diverted to biomass. This value ranges from 0 (no diversion) to 0.5 (half of all carbon lost to biomass).

In the system:

- **Dark fermentation** consistently yields **2 mol of hydrogen**, unaffected by biomass diversion.
- **Photofermentation** ideally yields **10 mol of hydrogen**, assuming all 4 remaining carbon atoms from glucose (after dark fermentation) are used to form butyric acid and are fully oxidized.

However, when biomass diversion occurs, fewer carbon atoms are available for oxidation in the photofermentation stage. Since 6 carbon atoms exist per glucose molecule and 2 are always released in dark fermentation, the remaining 4 are subject to diversion.

The number of available carbon atoms for photofermentation becomes: **4 – (6 × x)**

This means the actual photofermentation yield is: **10 × (available carbon ÷ 4) = 10 × (1 – 1.5x)**

Total hydrogen yield, combining both stages, is then: **H<sub>2</sub> yield = 2 + 10 × (1 – 1.5x)**

Which simplifies to: **H<sub>2</sub> yield = 12 – 15x**

**Final equation:**

**Adjusted hydrogen yield = 12 – 15 × BDF**

This equation assumes dark fermentation is constant, and photofermentation yield declines linearly with increasing biomass diversion.

### 9.3.2.2. Biological Realism Factor (BRF) Adjustment

These values can be combined with the Biomass Diversion Factor (BDF) for layered correction in scenario modelling. While BRF reflects metabolic inefficiencies even in optimized strains, BDF represents substrate diversion into biomass structures. Together, they define a more biologically constrained performance envelope.

## 9.4. Energy Yield Estimate

Each mole of hydrogen releases ~286 kJ of energy upon combustion. Based on 12 mol H<sub>2</sub> per glucose cycle:

- **Energy yield per mol glucose:**  $12 \times 286 = 3432 \text{ kJ}$ , or **~3.43 MJ**

This figure assumes complete combustion of hydrogen and no energy loss during storage or transfer.

## 10. Net Energy Balance and System Efficiency

To evaluate the practical viability of the proposed dual-stage microbial hydrogen production system, it is essential to quantify not only the theoretical energy output but also the energy required to operate the system components. This section outlines a preliminary energy balance based on stoichiometric hydrogen yield and estimated energy inputs under idealized bench-scale conditions.

### 10.1. Hydrogen Energy Output

Under ideal conditions, the system produces **12 mol of H<sub>2</sub>** per mole of glucose, resulting in a gross energy output of:

$$12 \text{ mol} \times 286 \text{ kJ/mol} = 3432 \text{ kJ (or } \sim 3.43 \text{ MJ)}$$

To reflect biological inefficiencies in enzyme expression and metabolic function, a **Biological Realism Factor (BRF)** is applied. BRF-scaled energy values are summarized in **Table 8.3.2**, alongside yield and efficiency adjustments. These corrected values define the system's expected energy ceiling under non-ideal operating conditions.

### 10.2. Estimated Energy Inputs

Energy inputs were estimated based on typical laboratory-scale setups and published literature. All values assume one full processing cycle (~24 hours) for 1 mole of glucose.

Component	Estimated Input (kJ)	Assumptions
LED Illumination (For Photofermentation)	600 kJ	~5–10 Watts LEDs over 24 hours
Vacuum-Assisted Gas Extraction	216 kJ	~30 Watts pump for 2 hours
Stirring, Control and pH regulation	144 kJ	6 Watts average load for 6 hours
Total Input Energy	960 kJ	

#### 10.2.1. Net Energy Gain and Efficiency

Under theoretical conditions, the system produces 3432 kJ of energy from hydrogen combustion and requires 960 kJ of energy to operate per cycle.

- **Net Energy Gain**

$$\text{Net Gain} = 3432 \text{ kJ (output)} - 960 \text{ kJ (input)} = 2472 \text{ kJ}$$

To quantify system performance, two different efficiency metrics are introduced:

**1. Energy Return on Input Energy (EROIE):** This reflects the sum of energy is recovered per unit of input energy.

$$\text{EROIE} = \frac{\text{Output Energy}}{\text{Input Energy}} = \frac{3432}{960} \approx 3.575$$

**2. Net Energy Fraction (NEF):** This represents the proportion of the **total energy cycle** that results in useful output.

$$NEF = \frac{\text{Output Energy}}{\text{Output} + \text{Input Energy}} = \frac{3432}{3432 + 960} \approx 0.7814 \text{ (or 78.14\%)}$$

**Clarification:** The term "system efficiency" is often misused in biological models. Here, both EROIE and NEF are reported to clarify different performance aspects:

- **EROIE** reflects viability from an energy investment perspective.
- **NEF** reflects how much of the total system energy remains in usable form.

### 10.3. Real-World Expectations

While the theoretical efficiency approaches 80%, practical efficiencies are expected to be lower. A biomass yield penalty of 5–10% is typically observed in practical systems due to resource allocation toward microbial maintenance and division. This was excluded from the current energy model to isolate system performance potential. Based on operational inefficiencies, microbial kinetics, and engineering limitations, **realistic system efficiency may range between 40–60%**. Factors influencing actual performance include:

- Partial pressure and selectivity losses in membrane separation
- Biofilm detachment or overgrowth
- Incomplete substrate conversion
- Heat loss and energy dissipation in control systems.
- LED degradation and photon scattering inefficiencies.

These must be addressed in future experimental trials and lifecycle assessments.

#### 10.3.1. Summary and Comparative Outlook

Metric	Value
H <sub>2</sub> Output (12 mol)	3432 kJ (3.43 MJ)
Estimated Input Energy	960 kJ
Net Energy Gain	2472 kJ
Idealized System Efficiency	~78.1%
Expected Real Efficiency	40–60% (projected)

This energy model provides a foundational benchmark for the future development of a scalable, energy-positive, microbial hydrogen platform. Further refinements will require integration with kinetic modelling, pilot-scale data, and dynamic energy budgeting across varying reactor designs.

#### 10.3.2. Clarifying Efficiency Metrics: Separation Loss vs. Total System Efficiency

The paper currently references two distinct ranges for practical energy efficiency:

- **67–72% efficiency** — reflecting only gas separation penalties and membrane inefficiencies under ideal microbial performance.
- **40–60% efficiency** — reflecting full-system inefficiencies including microbial losses, biomass diversion, expression instability, and light/mass transfer limitations.

*Clarification:* These ranges are not contradictory but represent **different layers of system constraint**.

To resolve potential confusion, the following delineation is made:

Efficiency Scope	Description	Estimated Range
<b>Gas-Adjusted Efficiency</b>	Accounts for membrane inefficiencies and gas separation penalties (e.g., 8% loss from 92% H <sub>2</sub> recovery)	<b>67–72%</b>
<b>Biology-Adjusted Efficiency</b>	Includes gas losses <b>plus</b> microbial inefficiencies such as ATP shortfalls, cofactor scarcity, biomass diversion, and yield throttling	<b>40–60%</b>
<b>Theoretical Max (NEF)</b>	Net energy fraction under idealized operation	<b>~78.1%</b>

The higher value (67–72%) assumes microbes operate near their theoretical ceiling, and the only losses occur in **gas handling**.

The lower value (40–60%) reflects **real-world biological constraints** such as:

- BRF-adjusted expression losses
- Biomass carbon diversion (BDF)
- ATP or cofactor bottlenecks
- Incomplete substrate conversion

*Conclusion:* When quoting system efficiency, it is essential to specify which domain the losses originate from. Future empirical models should separately quantify:

- Engineering penalties (e.g., membrane loss, pump inefficiency)
- Biological penalties (e.g., yield suppression, carbon retention) to provide a more precise picture of overall energy performance.

---

## Gas Separation Penalty

Real-world membrane systems rarely achieve perfect separation. With a hydrogen recovery efficiency of ~92% and vacuum pump efficiency of ~90%, two energy penalties must be considered:

- **Hydrogen Loss (~275 kJ):** Due to unrecovered hydrogen molecules during membrane passage, reducing usable gas output.
- **Vacuum Operation Cost (~216 kJ):** Represents the power required to run the vacuum pump, even under efficient cycling.

Together, these factors reduce the theoretical energy output of 3432 kJ per cycle by a total of ~491 kJ, resulting in an adjusted net energy gain of ~1960–2200 kJ, depending on membrane and vacuum system efficiency. This corresponds to a practical energy efficiency of **67–72%**, compared to the theoretical maximum of 78.1%.

These adjustments reinforce the importance of staged membrane arrays, fouling resistance, and supplemental polishing technologies (e.g., PSA or desiccant traps) for maintaining fuel-grade output.

## Clarified Statement on Gas Separation Losses and Energy Penalty

In the original model, the energy penalty from gas separation was expressed as a drop in usable hydrogen energy—from 3432 kJ (theoretical) to ~3157 kJ (realistic), amounting to an 8% loss. This value includes **both the loss of hydrogen due to imperfect membrane selectivity** (typically 5–10% unrecovered gas) and the **energy required to operate the vacuum extraction system** (216 kJ per cycle based on 30W pump usage for 2 hours).

It is important to distinguish between these two contributors:

- **Gas Loss Penalty (~274 kJ):** Represents the portion of hydrogen that diffuses inefficiently or is unrecovered during membrane separation.
- **Vacuum Energy Cost (216 kJ):** Represents the energetic overhead of powering the extraction system.

## Clarification on Energy Penalty Attribution:

The total energy penalty from the gas separation system is composed of **two distinct components** that must be treated separately:

1. **Hydrogen Loss Penalty (~275 kJ):** This represents the *reduction in usable energy output* due to membrane inefficiency—i.e., hydrogen gas that escapes capture and is therefore unavailable for combustion.
2. **Vacuum Pump Energy Input (~216 kJ):** This is an **operational energy cost**, representing the **power required** to run the membrane extraction system during gas separation.

These values should **not be combined into a single energy loss from the output stream**, as they affect different sides of the energy balance equation:

- The hydrogen loss **reduces gross energy output**:  
3432 kJ → 3157 kJ usable H<sub>2</sub> energy.
- The vacuum pump cost **adds to system input energy**:  
Total input = 960 kJ (including 216 kJ from vacuum system)

Therefore, the **net energy gain** remains:

- Net energy = 3157 – 960 = 2197 kJ
- **Real-world system efficiency ≈ 64% (2197 / 3432)**

This refined breakdown avoids double-counting and accurately distinguishes between **energy losses due to system inefficiency** and **energy costs due to system operation**.

*Side Note:* Yield values assuming 10 mol H<sub>2</sub> from photofermentation reflect a best-case ATP supply scenario. Under energy-limited conditions, ATP throttling may reduce this to 7.5–9 mol, resulting in cycle yields of ~9.5–11 mol H<sub>2</sub> and a corresponding drop in energy output and system EROIE.

## 11. Production Rate and Daily Throughput

To contextualize the system's practicality and operational output, this section presents a normalized daily breakdown of production, energy output, and carbon emissions based on a complete reactor cycle duration of 72 hours (3 days).

### 11.1. Cycle Duration Justification

The proposed system operates through a sequential two-stage microbial process:

#### 11.1.1. Stage 1: Dark Fermentation (*Clostridium butyricum*)

- Converts glucose into hydrogen and volatile fatty acids (VFAs)
- Doubling time: ~3–6 hours
- Hydrogen production typically peaks at 18–24 hours post-inoculation.
- Full substrate conversion is generally achieved within 24 hours in batch mode.

#### 11.1.2. Stage 2: Photofermentation (*Rhodobacter sphaeroides*)

- Converts VFAs into additional hydrogen via nitrogenase-driven metabolism.
- Process is light-dependent and slower.
- Photofermentation typically requires 2–5 days depending on light intensity and VFA concentration.
- Butyric acid breakdown extends total time requirements.

Based on this information, the full operating cycle is reasonably assumed to require approximately **72 hours (3 days)**.

### 11.2. Daily Breakdown of Core Outputs

Parameter	Per Cycle (3 Days)	Per Day (Averaged)
Hydrogen Output	12 mol	4 mol
Energy Output	3432 kJ	1144 kJ
Hydrogen Volume (STP)	~269 L	~89.7 L
CO <sub>2</sub> Emitted	6 mol	2 mol
CO <sub>2</sub> Mass	264 g	88 g
Glucose Consumed	180.16 g	60.05 g
Operational Cost	\$0.637	~\$0.212

*Side Note:* Hydrogen volume assumes STP = 22.4 L/mol at 0°C and 1 atm. Real values may vary depending on operational temperature and pressure.

### 11.3. Hydrogen Productivity Rate (Volume-Based)

Assuming a 2-litre total working reactor volume:

- **Hydrogen output/day** = 89.7 L / 2 L = **44.85 L H<sub>2</sub> per litre of reactor per day**
- **Energy output/day** = 1144 kJ / 2 L = **572 kJ per litre per day**

These values represent an idealized productivity scenario under fully optimized and stable microbial activity. Real-world rates may vary based on inoculum density, substrate purity, light intensity, and ambient conditions.



---

**Note on Gas Volume Calculations:**

All hydrogen volume values in this paper are calculated assuming **Standard Temperature and Pressure (STP)** defined as:

- **0°C (273.15 K)**
- **1 atm pressure (101.325 kPa)**
- **Molar volume of 22.4 L/mol**

If operating conditions differ (e.g., 25°C or pressurized storage), gas volume may vary accordingly. For precision applications, corrected volumes using the Ideal Gas Law or real gas equations should be applied.

---

## 11.4. Microbial Biomass Yield Efficiency

Literature on *Clostridium butyricum* batch fermentation systems commonly report dry biomass concentrations ranging from **1.0 to 3.0 g/L**, depending on substrate load, nutrient availability, and anaerobic conditions. For this model, a conservative estimate of **2.0 g/L** was assumed, consistent with OD<sub>600</sub> values of ~1.5–2.0 reported in microbial hydrogen production studies.

Assuming a working bioreactor volume of **2 litres**—representative of a lab-scale system operating at full aqueous capacity—the total microbial dry biomass is estimated at **4.0 grams**. Under these conditions, the reactor yields:

- **1.0 mol H<sub>2</sub> per gram of biomass per day**
- **0.5 mol CO<sub>2</sub> per gram of biomass per day**

This productivity aligns with the theoretical ceiling. Literature reports 0.15–0.75 mol/g/day depending on strain and light conditions. This model assumes optimized conditions and gene stack expression without metabolic burden.

*Side Note:* This system-wide production rate of ~4 mol H<sub>2</sub>/day corresponds to a microbial biomass concentration of 2 g/L across 2 L of working volume. At this biomass level, approximately 5–15% of substrate carbon is redirected toward cellular material. This supports the application of a Biomass Diversion Factor in overall yield and energy calculations (see Section 8.2.2). Section 9.4 provides the biomass-normalized rates derived from this same baseline (1.0 mol H<sub>2</sub>/g biomass/day and 0.5 mol CO<sub>2</sub>/g biomass/day), ensuring direct alignment between overall gas output and microbial load.

## 11.5. Implications for Scale-Up

This daily throughput model allows for direct scalability calculations. For example:

- A 100-litre reactor system (assuming same conditions) would yield:
  - ~8.97 m<sup>3</sup> H<sub>2</sub>/day
  - ~114.4 MJ/day
  - ~8.8 kg CO<sub>2</sub>/day

Such normalized values are essential for evaluating deployment potential across decentralized grids, small-scale industrial applications, or off-grid energy systems with integrated carbon management strategies.

## 12. CO<sub>2</sub> Redirection to Passive Sugarcane Sink

To ensure net-zero emissions and maintain the system's carbon-neutral profile, the carbon dioxide produced by microbial metabolism is redirected into a **dedicated sugarcane greenhouse or plantation pod** adjacent to the reactor setup.

### 12.1. Daily CO<sub>2</sub> Emissions

Based on stoichiometric fermentation pathways, the system emits:

- **6 mol CO<sub>2</sub> per cycle = 264 g CO<sub>2</sub> per 3 days**
- **Average per day = 2 mol CO<sub>2</sub> ≈ 88 grams/day**

### 12.2. Sugarcane CO<sub>2</sub> Fixation Capacity

Sugarcane is a high-efficiency **C<sub>4</sub> photosynthetic crop** known for rapid carbon uptake.

- Literature indicates sugarcane can fix **~666 g CO<sub>2</sub> per kg of biomass produced**.
- Required CO<sub>2</sub> offset: 88 g/day.

Required sugarcane growth per day:

$$\frac{88 \text{ g}}{666 \text{ g/kg}} \approx 0.132 \text{ kg} = 132 \text{ g sugarcane/day}$$

This requirement is modest and achievable in a small indoor greenhouse pod or planter-scale setup, especially under controlled light and nutrient conditions. Even minimal vegetative growth is sufficient to fully offset the reactor's daily CO<sub>2</sub> emissions.

#### 12.2.1. Why Sugarcane?

Sugarcane offers two-fold advantages:

1. **Exceptional CO<sub>2</sub> fixation** due to its C<sub>4</sub> metabolic pathway
2. **Glucose-rich stalks** make it a compatible future feedstock for microbial fermentation.

This symbiotic potential means that the same crop used for carbon offset could eventually be harvested to support future reactor cycles, contributing to a **semi-closed bioresource loop**.

### 12.3 Temporal Dynamics of CO<sub>2</sub> Fixation

While the daily CO<sub>2</sub> emission from microbial fermentation is estimated at ~88 g/day, the corresponding fixation by sugarcane biomass (~132 g/day growth for offset) assumes a smoothed average over an extended photoperiod and seasonal cycle. Sugarcane growth is not linear or instantaneous; it follows diurnal patterns and growth-phase-dependent rates influenced by light exposure, nutrient levels, and ambient conditions.

Therefore, the CO<sub>2</sub> fixation rate cited here represents an **averaged sequestration benchmark**, not a real-time sink. In practice, temporal mismatches between gas production and biological absorption may occur—particularly during early germination, cloudy periods, or seasonal dormancy.

To mitigate these mismatches, future designs could incorporate:

- **Buffer tanks** to store CO<sub>2</sub> until peak uptake hours.
- **Multi-species sink systems** (e.g., algae + sugarcane) for temporal balancing.
- **Monitoring and throttle protocols** based on plant health and CO<sub>2</sub> levels.

This correction ensures the system's carbon neutrality is evaluated on a **rolling timescale**, not instantaneously. Accurate life-cycle sequestration tracking is essential for long-term deployment and ecological verification.

---

### Author's Note: The Industrial Concern

While this model proposes a sustainable and ecologically integrated CO<sub>2</sub> management strategy, it is important to acknowledge a concern: **industrial-scale implementations may not uphold the passive offset system**. For economic or spatial reasons, CO<sub>2</sub> redirection could be bypassed or ignored, undermining the environmental integrity of the design.

Therefore, responsible implementation must treat CO<sub>2</sub> fixation as a **non-optional component**, not merely a sustainability add-on. Without it, the system reverts to a net-positive carbon emitter, contradicting its intended purpose.

### 13. CO<sub>2</sub> Sink Implementation and Maintenance Considerations

The efficacy of the proposed microbial hydrogen production system relies not only on hydrogen output but also on the successful redirection and neutralization of byproduct CO<sub>2</sub>. This section addresses the physical deployment, delivery method, and oversight mechanisms associated with the sugarcane-based carbon sink.

#### 13.1. Physical Setup: Sugarcane Pod Location

The sugarcane plants are assumed to be grown within a **dedicated greenhouse pod or adjacent indoor soil-based chamber**. This setting allows for year-round growth under controlled temperature, humidity, and light conditions. Soil-based planting is prioritized over hydroponics to simplify nutrient cycling and reduce technological overhead. The pod is spatially integrated to minimize gas transfer distance.

#### 13.2. CO<sub>2</sub> Transfer Mechanism

CO<sub>2</sub> generated during fermentation is captured via membrane separation and routed into the sugarcane pod through **low-pressure, gas-tight tubing**. Dispersion strategies include:

- **Atmospheric diffusion:** Gas is released into the plant chamber for natural absorption.
- **Root-zone injection:** CO<sub>2</sub> is directed into soil channels for partial dissolution and uptake.

For bench-scale systems, passive atmospheric mixing is likely sufficient.

#### 13.3. Maintenance and Oversight

To prevent CO<sub>2</sub> buildup due to plant failure or neglect, future-scale systems may include:

- **CO<sub>2</sub> sensors** in the exhaust loop or pod
- **Automatic throttling or shutdown** if CO<sub>2</sub> thresholds are exceeded.
- **Optional health monitoring** of sugarcane growth using basic spectral sensors.

These features ensure carbon sequestration remains enforced, not optional.

#### 13.4. Ethical and Industrial Caution

While the passive CO<sub>2</sub> sink model is designed for simplicity and reliability, there is a tangible risk that industrial-scale adopters may attempt to omit or disable the sequestration component to reduce costs or footprint. Such practices would fundamentally undermine the system's sustainability claims and revert it to a net-emitter.

To avoid this outcome, system deployment should be guided by strict sustainability protocols that include the carbon sink as a **non-optional element** of the hydrogen production framework. Long-term success hinges not only on microbial efficiency, but also on upholding the environmental intent of the design.

## 14. Kinetic Considerations and Theoretical Modelling Framework

### 14.1. Objective of Kinetics Modelling

While stoichiometric analysis provides a snapshot of theoretical yield, it lacks the temporal resolution required to optimize real-world reactor performance. Kinetic modelling addresses this gap by characterizing the **rate at which biochemical transformations occur** under varying environmental and operational conditions.

In the context of this dual-stage microbial hydrogen system, kinetics modelling serves the following key purposes:

- **Predicting hydrogen production rates** over time for each microbial stage
- **Identifying limiting factors**, such as substrate saturation, product inhibition, or light flux variability
- **Optimizing substrate feeding strategies** to avoid bottlenecks or microbial shock
- **Enabling scale-up modelling** through time-dependent simulations of batch and continuous systems
- **Supporting future automation** by providing a framework for real-time feedback control

By introducing kinetic parameters into the system framework, the model transitions from a static yield estimate to a dynamic, time-resolved process capable of iterative refinement and control.

### 14.3. Dark Fermentation Kinetics (*Clostridium butyricum*)

The dark fermentation stage, facilitated by *Clostridium butyricum*, is responsible for the initial conversion of glucose into hydrogen and volatile fatty acids (VFAs). This process can be described using **Monod kinetics**, which relate microbial growth or substrate consumption rate to substrate concentration:

$$r = r_{max} \frac{[S]}{K_s + [S]}$$

Where:

- $r$ : Rate of glucose consumption or hydrogen production
- $r_{max}$ : Maximum rate under saturated conditions
- $[S]$ : Substrate concentration (glucose)
- $K_s$ : Half-Saturation constant

In specific conditions, substrate inhibition may occur at high glucose concentrations. This can be modelled by extended forms such as the **Haldane equation** to reflect non-linear inhibition kinetics.

#### 14.3.1. Example Calculation using Empirical Parameters

Based on reported kinetic data for *Clostridium butyricum*, the following parameters were selected for modelling hydrogen production via *Monod kinetics* [Khanal et al., 2018]:

- $r_{max} = 14.92 \text{ day}^{-1}$  (max growth rate)
- $K_s = 1.02 \text{ g COD/L}$  (substrate affinity)
- $[S] = 1.5 \text{ g COD/L}$  (Glucose feed concentration assumed)

Substituting into Monod equation:

$$r = 14.92 \times \frac{1.5}{1.02 + 1.5} = 14.92 \times 0.595 = 8.87 \text{ day}^{-1}$$

Thus, under these conditions, the system achieves a glucose-specific growth rate of **8.87 day<sup>-1</sup>**, indicating strong substrate utilization.

[Source:] Khanal, S. K., et al. (2018). *Kinetic modelling and microbial community analysis for high-rate hydrogen production in a dynamic membrane bioreactor*. [PubMed](#)

#### 14.4. Photofermentation Kinetics (*Rhodobacter sphaeroides*)

Due to the lack of real-time experimental data for photofermentation kinetics, light-saturation modelling is presented using standard literature values for similar strains under ideal lab conditions. These values are included solely for theoretical demonstration.

The second stage involves *Rhodobacter sphaeroides*, which uses VFAs produced during dark fermentation to generate additional hydrogen via photofermentation. This process is primarily limited by **light intensity** and substrate availability. The rate of hydrogen production can be approximated using light-dependent kinetics:

$$r = r_{max} \frac{I}{K_I + I}$$

Where:

- $I$ : Incident light intensity ( $\mu\text{mol photons/m}^2/\text{s}$ )
- $K_I$ : Light saturation constant

In addition to light, nitrogenase enzyme activity and VFA accumulation influence the overall rate. Optimization may require tuning light exposure profiles and avoiding product buildup that inhibits microbial metabolism.

##### 14.4.1. Example Calculation using Empirical Parameters

Light-dependent kinetics of *Rhodobacter sphaeroides* were modelled using data from *Thaiwong et al. (2015)*, which report:

- Optimal light intensity: 7500 lux
- $r_{max} = \sim 12.0 \text{ ml H}_2/\text{L} \cdot \text{h} = 0.288 \text{ mol H}_2/\text{L/day}$
- $K_I$  (Estimated light half-saturation constant):  $\sim 4500 \text{ lux}$ .

Assuming light intensity  $I = 6000$  lux:

$$r = 0.288 \times \frac{6000}{4500 + 6000} = 0.288 \times 0.571 = 0.164 \text{ mol } H_2/L/day$$

This rate reflects mid-range illumination conditions achievable in bioreactor systems with LED panels.

**[Source:]** Thaiwong, N., et al. (2015). *Photo-fermentational hydrogen production of Rhodobacter sp. KKU-PS1 under various illumination intensities*. [SciELO](#)

*Side Note:* These empirical parameters are context-dependent and vary based on reactor design, inoculum age, and light delivery systems. They are presented here to demonstrate integration of real-world kinetics into the model framework.

## 14.5. Coupled Kinetic Modelling

To simulate the full dual-stage reactor dynamically, the two microbial stages can be coupled in a sequential or semi-continuous configuration. The output of the first stage (VFAs) becomes the input substrate for the second stage. An **ODE-based model** can be constructed to track glucose degradation, VFA production, and hydrogen evolution over time:

- Let  $G(t)$ : Glucose concentration over time.
- Let  $V(t)$ : Volatile fatty acid concentration.
- Let  $H(t)$ : Hydrogen yield curve.

Differential equations can describe rates of change in each metabolite pool and be fitted using experimental time-course data in future implementations.

## 14.6. Limitations and Future Directions

While the proposed kinetic framework outlines a theoretical basis for dynamic system modelling, it currently lacks empirical validation. Parameters such as  $K_s$ ,  $K_I$ , and  $r_{max}$  are not specified due to the absence of real-time growth or yield curve data. Future experimental studies are needed to:

- Calibrate model parameters using actual fermentation trials.
- Validate system response to variable substrate concentrations and light conditions.
- Develop predictive tools for system control and optimization.

These kinetic models are not intended as predictive tools in their current form. Rather, they provide a foundation for rate-dependent system refinement once empirical data becomes available.

Nonetheless, the inclusion of a kinetic modelling framework establishes the groundwork for advancing this hydrogen production system toward real-time performance tuning and intelligent reactor control.

## 15. Cost Efficiency Estimate and Benchmarking

To assess economic feasibility, an approximate cost breakdown was developed for a single hydrogen production cycle under bench-scale operation, assuming U.S.-based pricing standards [6,7].

### 15.1. U.S. Cost Assumptions:

- **Electricity:** \$0.10 per kWh (industrial rate)
- **Glucose (bulk, biotech-grade):** ~\$2 per kg
- **Membrane unit:** \$100, amortized over 500 cycles.

### 15.2. Cost Breakdown per Cycle (1 mol glucose processed):

Item	Cost per Cycle (USD)	Notes
Electricity (0.267 kWh)	\$0.027	960 kJ input total
Glucose (180.16 g)	\$0.36	Based on \$2/kg bulk rate
Membrane amortization	\$0.20	\$100 module over 500 cycles
Nutrients, buffers, misc.	\$0.05	Estimated buffer cost
<b>Total</b>	<b>\$0.637</b>	

*Side Note:* This cost does not include polishing units or membrane cleaning cycles. If membrane lifetime drops below 300 cycles due to fouling or efficiency loss, per-cycle costs increase to ~\$0.33, with added energy penalties for vacuum inefficiency and purity upgrades.

### 15.3. Cost per Energy Unit:

Based on the total operational cost of **\$0.637 per cycle**, the system's theoretical cost efficiency can be calculated relative to hydrogen energy output.

At the theoretical maximum (12 mol H<sub>2</sub>), the system yields **3.43 MJ** of energy:

Cost per MJ H<sub>2</sub> = \$0.637 / 3.43 ≈ **\$0.186/MJ**

Cost per mol H<sub>2</sub> = \$0.637 / 12 mol ≈ **\$0.053/mol H<sub>2</sub>**

To incorporate metabolic inefficiencies, the **Biological Realism Factor (BRF)** is applied to simulate performance under non-ideal conditions:

BRF	Energy Output (MJ)	H <sub>2</sub> Yield (mol)	Cost per MJ (\$)	Cost per mol H <sub>2</sub> (\$)
1.00	3.43	12.0	0.186	0.0531
0.90	3.08	10.8	0.207	0.0590
0.80	2.75	9.6	0.232	0.0663
0.75	2.57	9.0	0.248	0.0708

These figures highlight how **cost efficiency degrades** as enzyme activity and metabolic performance fall short of ideal. The rise in cost per MJ reflects reduced hydrogen recovery, even though per-cycle expenses remain constant. This reinforces the importance of **genetic stability**, **expression fidelity**, and **process control** in maintaining economically viable operation.



## 16. Comparative Cost of Hydrogen Production Methods:

To contextualize the cost-effectiveness of the proposed system, the following table compares the theoretical model with conventional and emerging hydrogen production methods based on published estimates.

Method	Cost per MJ H <sub>2</sub>	Cost per Mole H <sub>2</sub>	CO <sub>2</sub> Emissions	Energy Efficiency	Notes
<b>This Model (Theoretical)</b>	<b>\$0.186</b>	<b>\$0.053</b>	Medium (recycled)	~78% (ideal)	Bench-scale, bio-based
Steam Methane Reforming (SMR)	\$0.80–\$1.00	~\$0.23–\$0.29	High (direct emissions)	~65–75%	Industrial standard
Water Electrolysis (Renewables)	\$0.50–\$1.50	~\$0.14–\$0.43	Low (if powered by renewables)	~50–70%	Dependent on clean grid
Biomass Gasification	\$0.40–\$0.60	~\$0.11–\$0.17	Medium (feedstock-dependent)	~60–70%	Requires preprocessing
Alkaline Electrolysis (Grid)	~\$1.20	~\$0.34	High (if fossil-powered)	~55%	Mature but energy-intensive

This comparison highlights the economic promise of biologically driven hydrogen production when paired with low-cost substrates and efficient CO<sub>2</sub> handling. Although these values are theoretical and do not yet include full system capital expenditure or operational overhead, the model suggests a strong potential for competitive deployment in decentralized, sustainable energy frameworks.

## Discussion

the potential for significantly higher theoretical hydrogen yields compared to conventional single-stage fermentation approaches. By coupling *Clostridium butyricum*-driven dark fermentation with *Rhodobacter sphaeroides*-based photofermentation, the model achieves a projected output of 12 mol H<sub>2</sub> per cycle, corresponding to 13.45% hydrogen by mass relative to glucose input, or 8.41% when including water. This yield exceeds the typical range reported for unoptimized single-stage systems, which average between 2–4 mol H<sub>2</sub>/mol glucose.

These results are based on several idealized assumptions, including near-complete substrate conversion, stable enzymatic activity, and minimal gas separation losses under optimal conditions. In practice, factors such as membrane fouling, product inhibition, and microbial fluctuations are likely to introduce performance variability. The system also assumes that genetically engineered strains express target modifications without loss of function, mutation, or metabolic interference. While such assumptions serve to establish an upper-bound performance model, real-world implementation will require extensive refinement to address system complexity and variability.

The inclusion of kinetic modelling offers deeper insight into microbial behaviour under dynamic conditions. By quantifying stage-specific reaction rates, the model allows for predictive simulations and real-time control strategies in future implementations. Furthermore, the carbon mitigation strategy, when paired with sensor-driven fail-safes, ensures that CO<sub>2</sub> sequestration remains an enforced requirement rather than an ethical suggestion. While the sugarcane-based sink is practical at bench scale, scalability will require protocol standardization to prevent industrial misuse or neglect.

In particular, the bioreactor architecture—though optimized on paper—presents multiple engineering challenges, including the stabilization of microbial biofilms, maintenance of anaerobic conditions, controlled light penetration, and non-intrusive gas extraction. The integration of vacuum-assisted membrane separation, while theoretically viable, must be evaluated against pressure regulation constraints, energy demands, and potential effects on microbial health and adhesion.

Furthermore, the CO<sub>2</sub> redirection strategy introduces its own set of complications. While biological sinks such as sugarcane, bamboo forests, and algae bioreactors offer promising carbon offset potential, their practical deployment is highly dependent on land use, climate, nutrient demand, and economic scalability. The feasibility of using CO<sub>2</sub> as a renewable feedstock hinge on localized resource availability and system compatibility, both of which remain unresolved in this theoretical model.

Despite these limitations, the study establishes a foundation for future work in genetically assisted, bioreactor-integrated hydrogen systems. It highlights key areas for experimental validation, including gene expression profiling, pathway stability, reactor material compatibility, and gas separation hardware design. Additional work is needed to model microbial kinetics, energy efficiency, and biofilm lifespan under continuous operation.

In summary, this model offers a high-yield conceptual framework for decentralized, carbon conscious hydrogen production, while acknowledging that practical application will require interdisciplinary advances in synthetic biology, bioprocess engineering, and environmental systems integration.

## **Scope of Integration and Original Contributions**

This study builds upon established research in microbial hydrogen production by proposing a dual-stage system that integrates dark and photofermentation, gas separation, and CO<sub>2</sub> fixation into a unified conceptual framework. While the individual components used are not novel, the specific arrangement and application context offer a potentially original contribution.

To the best of the author's knowledge, the following features are not currently documented in the literature as a single integrated system:

**(A)** While prior systems have explored dual-stage microbial hydrogen production, this reactor introduces gravity-fed passive transfer between stratified biofilms without active circulation, simplifying system mechanics while preserving metabolic continuity. This design seeks to simplify operational complexity while maintaining metabolic continuity.

**(B)** The coupling of microbial CO<sub>2</sub> emissions to a modular sugarcane-based carbon sink intended not only for sequestration, but for future glucose regeneration and system looping. While sugarcane is known for carbon capture, its role as a passive CO<sub>2</sub> sink within a microbial hydrogen system is, as far as the author is aware, not reported.

These features are presented as exploratory design contributions aimed at improving system modularity, passive control, and long-term sustainability. Further literature review and peer dialogue may reveal comparable systems, in which case this work still serves to formalize and extend such ideas in a structured, quantitative model.

While recent electrochemical DAC systems such as the fluo flavine-based redox sorbent (April 2025) demonstrate improved oxygen tolerance and partial reversibility, their lack of a defined downstream CO<sub>2</sub> utilization pathway severely limits practical integration. In contrast to biological systems, which inherently incorporate carbon fixation and valorisation (e.g., glucose synthesis, biomass generation), such redox DACs isolate CO<sub>2</sub> only to re-release it following energy-intensive regeneration. Without a metabolic or synthetic coupling mechanism, these systems risk functioning as carbon delay mechanisms rather than true sinks. The present architecture explicitly addresses this limitation by embedding CO<sub>2</sub> into a biological recycling loop via C<sub>4</sub> plant integration and microbial fermentation, enabling a closed carbon-energy cycle that produces usable hydrogen gas as output. The system presented here treats CO<sub>2</sub> not as waste to be held, but as a **metabolic resource to be converted**—a distinction absent from non-valorised DAC implementations. In short, capture without transformation does not constitute mitigation.

## Conclusion

This paper has outlined a theoretical dual-stage microbial hydrogen production system combining dark fermentation by *Clostridium butyricum* with photofermentation by *Rhodobacter sphaeroides*. By leveraging genetically optimized strains and integrating CO<sub>2</sub> redirection to high-efficiency sinks, the model achieves a theoretical ceiling of 12 mol H<sub>2</sub> per glucose cycle—equivalent to ~3.43 MJ of energy.

Key architectural features, including scaffolded biofilms, vacuum-assisted gas separation, and modular environmental control systems, are designed to maximize yield under idealized conditions. The framework introduces correction factors such as the Biological Realism Factor (BRF) and Biomass Diversion Factor (BDF) to adjust for non-ideal behaviour, offering a spectrum of operational outcomes from best-case scenarios to realism-aligned estimates.

Despite its theoretical robustness, the model acknowledges several unresolved challenges:

- Enzyme inhibition under H<sub>2</sub> accumulation
- Genetic stack incompatibility and regulatory crosstalk
- ATP insufficiency in photofermentation stages
- Realistic gas separation throughput and purity demands.

The proposed system serves as a conceptual benchmark rather than a blueprint for immediate deployment. It establishes an upper-bound performance envelope for decentralized biohydrogen generation and invites further empirical testing, kinetic modelling, and bioreactor optimization. The goal is to inform scalable, sustainable alternatives to fossil-fuel-derived hydrogen—rooted in biological efficiency and circular carbon integration.

## **Future Work**

To transition this theoretical framework into an experimentally validated system, the following research directions are recommended:

### **Empirical Validation of Genetic Stacks**

- Evaluate individual and stacked gene edits in *C. butyricum* and *R. sphaeroides* for stability, yield, and ATP burden under continuous culture.

### **Dynamic ATP Budget and Cofactor Modelling**

- Apply flux balance analysis (FBA) or dFBA to quantify resource allocation and identify limiting nodes in the energy network, particularly for nitrogenase ATP demands.

### **Photofermentation Surface Area Optimization**

- Simulate light attenuation in 3D biofilm geometries to determine minimum surface area per litre for optimal yield, especially under low-light or compact designs.

### **Headspace Gas Kinetics and Inhibition Prevention**

- Model partial pressure build-up, membrane throughput, and gas removal rates in real time to prevent enzymatic feedback inhibition.

### **Pilot-Scale Bioreactor Prototyping**

- Construct and evaluate a benchtop or microfluidic version of the dual-chamber reactor with real gas separation and CO<sub>2</sub> routing to verify assumptions on yield, thermal stability, and biofilm integrity.

### **CO<sub>2</sub> Sink Responsiveness and Climate Sensitivity**

- Evaluate how sugarcane, algae, or bamboo sinks perform under varied climate zones, soil conditions, and CO<sub>2</sub> loading rates, and simulate adaptive control loops.

These tasks will determine the feasibility of translating theoretical yields into real-world outputs, guiding the development of robust, decentralized hydrogen systems for energy resilience and climate alignment.

## Proposed Model Extensions for Future Work

This table outlines key limitations of the current theoretical framework, and the recommended extensions needed for more realistic, dynamic, or industrial-scale simulations. Each entry includes the limiting factor, the proposed modelling solution, and the relevant computational or experimental tool required.

Current Limitation	Proposed Extension	Required Tool / Method	Implementation Target
Static stoichiometric model	Add dynamic flux-based modelling (e.g., dFBA)	Flux Balance Analysis (COBRApy, FAME)	Sections 3, 4
No intracellular ATP tracking	Simulate ATP generation/consumption flux	Constraint-based kinetic modelling	Section 4.4.1
Headspace pressure not modelled	Time-dependent gas accumulation curve	Ideal gas law + Fick's law ODEs	Section 5.3.1
Membrane flow is idealized	Add fouling rates, permeability decay curves	Empirical correction factors or CFD	Section 5.3.1
Cofactor limitation (Fe, Mo, NAD(P)H) ignored	Mass balance of metal uptake & enzyme kinetics	Metal transport ODEs / SBML	Section 4.4.2
Gene stack synergy assumed	Model transcriptomic burden and ribosome load	Gene regulatory network simulation	Section 4.4.4
Light flux treated as uniform	Photon distribution and shadow mapping	Ray-trace modelling or photonic mesh	Section 5.2.2
Redox imbalance unaccounted for	NADH/NADPH pool flux tracking	Coupled redox and energy models	Section 4.4.3
No carbon/nutrient recycling loop modelled	Include feedback from CO <sub>2</sub> sink performance	Coupled biogeochemical cycle model	Sections 3.4, 2.6

The model's modular architecture allows these extensions to be implemented progressively. Future iterations will prioritize dynamic ATP modelling, trace metal limitations, and integrated pressure control simulations as first-tier improvements.

Future implementation will incorporate COBRApy-based FBA simulations or similar genome-scale constraint solvers for *Clostridium* and *Rhodobacter* strains to dynamically resolve flux bottlenecks under BRF and GSCF regimes.

## References

- [1] Khanal, S. K., et al. (2018). Kinetic modelling and microbial community analysis for high-rate hydrogen production in a dynamic membrane bioreactor. [Process for the successive production of calcium galactonate crystals by \*Gluconobacter oxydans\* - ScienceDirect](#)
- [2] Thaiwong, N., Reungsang, A., & Plangklang, P. (2015). Photo-fermentational hydrogen production of *Rhodobacter* sp. KCU-PS1 under various illumination intensities. [Stable expression and characterization of a fungal pectinase and bacterial peroxidase genes in tobacco chloroplast - ScienceDirect](#)
- [3] Hallenbeck, P. C., & Ghosh, D. (2009). [Advances in fermentative biohydrogen production: the way forward? Trends in Biotechnology](#) , 27(5), 287–297
- [4] McKinlay, J. B., & Harwood, C. S. (2010). Photobiological production of hydrogen gas as a biofuel. *Current Opinion in Biotechnology*, 21(3), 244–251. [Plant biotechnology - ScienceDirect](#)
- [5] Bernardo, P., Drioli, E., & Golemme, G. (2009). [Membrane Gas Separation: A Review/State of the Art | Industrial & Engineering Chemistry Research](#), 48(10), 4638–4663.
- [6] U.S. Department of Energy. (2023). Hydrogen Production: Electrolysis and Thermochemical Methods. [Hydrogen Production | Department of Energy](#)
- [7] International Energy Agency. (2019). *The Future of Hydrogen: Seizing today's opportunities*. [The Future of Hydrogen – Analysis - IEA](#)
- [8] Ghosh, S., & Hallenbeck, P. C. (2010). [Advances in fermentative biohydrogen production: the way forward? - PubMed](#) Trends in Biotechnology, 28(10), 531–538.
- [9] Nath, K., & Das, D. (2004). [Improvement of fermentative hydrogen production: various approaches - PubMed](#) Applied Microbiology and Biotechnology, 65, 520–529.
- [10] Wei et al. (2025). [Electrochemically induced carbon dioxide capture from air with an aqueous fluoquinone sorbent | Materials Chemistry | ChemRxiv | Cambridge Open Engage](#)
- [11] Morimoto, M. et al. (2004). [Biological production of hydrogen from glucose by natural anaerobic microflora - ScienceDirect](#)